AFRL-RX-WP-TP-2008-4321

LOW-TEMPERATURE COARSENING AND PLASTIC-FLOW BEHAVIOR OF AN ALPHA/BETA TITANIUM BILLET MATERIAL WITH AN ULTRAFINE MICROSTRUCTURE (PREPRINT)

G.A. Sargent, A.P. Zane, P.N. Fagin, A.K. Ghosh, and S.L. Semiatin

Metals Branch
Metals, Ceramics, and NDE Division

APRIL 2008

AIR FORCE RESEARCH LABORATORY
MATERIALS AND MANUFACTURING DIRECTORATE
WRIGHT-PATTERSON AIR FORCE BASE, OH 45433-7750
AIR FORCE MATERIEL COMMAND
UNITED STATES AIR FORCE

REPORT DOCUMENTATION PAGE

Form Approved
OMB No. 0704-0188

1. REPORT DATE *(DD-MM-YY)*	2. REPORT TYPE	3. DATES COVERED *(From - To)*
April 2008	Journal Article Preprint	

4. TITLE AND SUBTITLE

LOW-TEMPERATURE COARSENING AND PLASTIC-FLOW BEHAVIOR OF AN ALPHA/BETA TITANIUM BILLET MATERIAL WITH AN ULTRAFINE MICROSTRUCTURE (PREPRINT)

5a. CONTRACT NUMBER
In-house

5b. GRANT NUMBER

5c. PROGRAM ELEMENT NUMBER
62102F

6. AUTHOR(S)

G.A. Sargent (University of Dayton)
A.P. Zane (Wright State University)
P.N. Fagin (UES, Inc.)
A.K. Ghosh (University of Michigan)
S.L. Semiatin (AFRL/RXLMP)

5d. PROJECT NUMBER
4347

5e. TASK NUMBER
RG

5f. WORK UNIT NUMBER
M02R2000

7. PERFORMING ORGANIZATION NAME(S) AND ADDRESS(ES)

University of Dayton
Wright State University
UES, Inc.
University of Michigan

Metals Branch (AFRL/RXLMP)
Metals, Ceramics, and NDE Division
Materials and Manufacturing Directorate
Wright-Patterson Air Force Base, OH 45433-7750
Air Force Materiel Command, United States Air Force

8. PERFORMING ORGANIZATION REPORT NUMBER
AFRL-RX-WP-TP-2008-4321

9. SPONSORING/MONITORING AGENCY NAME(S) AND ADDRESS(ES)

Air Force Research Laboratory
Materials and Manufacturing Directorate
Wright-Patterson Air Force Base, OH 45433-7750
Air Force Materiel Command
United States Air Force

10. SPONSORING/MONITORING AGENCY ACRONYM(S)
AFRL/RXLMP

11. SPONSORING/MONITORING AGENCY REPORT NUMBER(S)
AFRL-RX-WP-TP-2008-4321

12. DISTRIBUTION/AVAILABILITY STATEMENT
Approved for public release; distribution unlimited.

13. SUPPLEMENTARY NOTES
Journal article submitted to *Metallurgical and Materials Transactions A*. PAO Case Number: WPAFB 08-2929; Clearance Date: 15 Apr 2008. The U.S. Government is joint author of this work and has the right to use, modify, reproduce, release, perform, display, or disclose the work.

14. ABSTRACT

The influence of microstructure evolution on the low-temperature superplasticity of ultrafine alpha/beta titanium alloys was established. For this purpose, the static and dynamic coarsening response and plastic-flow behavior of Ti-6Al-4V with a submicrocrystalline microstructure were determined via a series of heat treatments and uniaxial compression tests at temperatures of 650, 775, and 815 °C at all test temperatures, static coarsening exhibited diffusion-controlled kinetics and followed a dependence on phase composition and volume fraction qualitatively similar to previous observations at 850 to 950 °C. Dynamic coarsening at 775 and 815 °C and strain rates was similar to prior higher temperature observations as well in that the kinetics were approximately on order of magnitude faster than the corresponding static behaviors. The increase in coarsening rate with superimposed deformation was attributed to the enhancement of diffusion by dislocations generated in the softer beta phase.

15. SUBJECT TERMS
titanium alloys, static coarsening, dynamic coarsening, superplasticity

16. SECURITY CLASSIFICATION OF:			17. LIMITATION OF ABSTRACT:	18. NUMBER OF PAGES	19a. NAME OF RESPONSIBLE PERSON (Monitor)
a. REPORT	b. ABSTRACT	c. THIS PAGE			Sheldon L. Semiatin
Unclassified	Unclassified	Unclassified	SAR	54	19b. TELEPHONE NUMBER *(Include Area Code)* N/A

Standard Form 298 (Rev. 8-98)
Prescribed by ANSI Std. Z39-18

LOW-TEMPERATURE COARSENING AND PLASTIC-FLOW BEHAVIOR OF AN ALPHA/BETA TITANIUM BILLET MATERIAL WITH AN ULTRAFINE MICROSTRUCTURE

G.A. Sargent*, A.P. Zane**, P.N. Fagin[§], A.K. Ghosh[‡], and S.L. Semiatin

Air Force Research Laboratory, Materials and Manufacturing Directorate, AFRL/MLLM, Wright-Patterson Air Force Base, OH 45433

* University of Dayton, 300 College Park, Dayton, OH 45409

** Chemistry Department, Wright-State University, Dayton, OH 45435

[§] UES, Inc., 4401 Dayton-Xenia Road, Dayton, OH 45432

[‡] Materials Science and Engineering Department, University of Michigan, Ann Arbor, MI 48109-2136

ABSTRACT

The influence of microstructure evolution on the low-temperature superplasticity of ultrafine alpha/beta titanium alloys was established. For this purpose, the static and dynamic coarsening response and plastic-flow behavior of Ti-6Al-4V with a submicrocrystalline microstructure were determined via a series of heat treatments and uniaxaial compression tests at temperatures of 650, 775, and 815°C. At all test temperatures, static coarsening exhibited diffusion-controlled (r^3-vs-time) kinetics and followed a dependence on phase composition and volume fraction qualitatively similar to previous observations at 850-950°C. *Dynamic* coarsening at 775 and 815°C and strain rates of 10^{-4} and 10^{-3} s^{-1} was similar to prior higher-temperature observations as well in that the kinetics were approximately one order of magnitude faster than the corresponding static behaviors. The increase in coarsening rate with superimposed deformation was attributed to the enhancement of diffusion by dislocations generated in the softer beta phase. With respect to deformation

response, plastic flow was superplastic with m values of ~0.6 at 650, 775 and 815°C and strain rates of 10^{-4} and 10^{-3} s^{-1}. Dynamic coarsening resulted in flow hardening at both temperatures and strain rates for a short preheat time (15 minutes) but was noticeably reduced when a longer preheat time (1 h) was used prior to testing at 10^{-3} s^{-1}. The latter behavior was largely attributed to noticeable static coarsening during preheating. A generalized constitutive relation based on a single stress exponent and the instantaneous alpha particle size was shown to describe the superplastic flow of ultrafine Ti-6Al-4V at low *and* high temperatures.
Keywords: titanium alloys, static coarsening, dynamic coarsening, superplasticity

I. INTRODUCTION

The development of severe-plastic-deformation (SPD) methods to produce ultrafine microstructures in bulk metallic materials has spurred considerable research into enhanced secondary forming response and service properties [1-3]. The vast majority of this work has focused on single-phase fcc or bcc alloys with or without second-phase particles. In general, these efforts have demonstrated the ability to produce materials with superplastic forming (SPF) behavior at lower temperatures and/or higher strain rates than those required for conventional, coarser-grain materials. Considerable increases in strength and at times an attractive balance of strength *and* ductility have also been achieved [4].

The SPD of more complex, two-phase alloys with a large fraction of second phase has received less attention. In part, this is due to the reduced workability of such materials at low processing temperatures and the special tooling required for both the SPD operation itself and the determination of final

SPF properties. Alpha/beta titanium alloys comprise such a material class for which low-temperature/high-strain rate SPF is particularly attractive [5, 6]. Reduced temperature (for example, from ~900°C to ~ 775°C) and higher forming rates would enable utilization of less expensive tooling materials (e.g., stainless steel rather than superalloys), faster cycle times, and reduced material losses and machining costs associated with part contamination (alpha case). The production of alpha/beta titanium alloys such as Ti-6Al-4V with an ultrafine microstructure is usually accomplished via a series of steps consisting of annealing above the beta transus temperature (at which alpha + beta $\rightarrow$ beta) and water quenching to develop a fine, martensitic-alpha microstructure followed by SPD at warm-working temperatures. In the past, SPD has been imparted by rolling of sheet [7], multi-directional ('abc') forging [8, 9], equal-channel angular extrusion [10], severe compression under superimposed hydrostatic pressure [11], and high-pressure torsion [12]. By this means, ultrafine Ti-6Al-4V having a strain rate sensitivity (m value) of the order of 0.35 - 0.65 and elongation between 400 and 1100 pct. at temperatures between 700 and 800°C has been produced.

Despite the success in developing ultrafine microstructures in alpha/beta titanium alloys, there are many unanswered questions regarding the mechanisms underlying low-temperature superplasticity of such materials. These include the kinetics of microstructural coarsening prior to and during deformation and the exact mechanism that controls superplasticity itself. It is well known that coarsening during deformation (i.e., dynamic coarsening) of alpha/beta titanium alloys with either a relatively coarse or ultrafine starting microstructure can lead

to noticeable flow hardening at conventional superplastic forming temperatures [13, 14]. The interrelation of coarsening and flow hardening is unknown for low-temperature deformation.

A quantitative micromechanical description of the superplastic flow of two-phase alloys such as Ti-6Al-4V poses a major challenge as well. The majority of previous work attempted to interpret observations in terms of models based on the deformation of single-phase alloys with fine equiaxed grain structures. In these models, stress concentrations developed at triple points due to grain-boundary sliding (gbs) are often assumed to be accommodated by climb-limited glide of dislocations in the vicinity of grain boundaries (i.e., mantle regions) or diffusional flow either through the grains or along the grain boundaries. The former explanation (climb-limited glide of dislocations), first proposed by Gifkins [15] and later extended by Ghosh [16], appears to be the most successful explanation of superplasticity. For example, based on observations of the sigmoidal dependence of stress σ and strain rate $\dot{\varepsilon}$ (plotted in logarithmic coordinates) over a wide strain-rate regime (both within and outside the superplastic range), Ghosh [16] developed a relation combining the individual contributions to plastic flow of grain-mantle ($\dot{\varepsilon}_M$) and grain-core ($\dot{\varepsilon}_C$) deformation, viz.:

$$\dot{\varepsilon} = \dot{\varepsilon}_M + \dot{\varepsilon}_C = (B/d^2)(\sigma-\sigma_o)^M + K\sigma^N, \qquad (1)$$

in which B and K are constants dependent on temperature and microstructure, d denotes the grain size, σ_o is the threshold stress, M is the stress exponent for mantle deformation, and N is the stress exponent for core (creep) deformation.

The application of two-mechanism models such as that of Ghosh [16] for the case in which concurrent coarsening occurs poses a major challenge. In such cases, a single-mechanism form is often utilized, primarily for a narrow strain-rate regime such as that characterized solely by superplastic flow. The most common of such generalized strain rate-stress relations is the following [17, 18]:

$$\dot{\varepsilon} = \left(\frac{ADGb}{kT}\right)\left(\frac{\sigma}{G}\right)^{n}\left(\frac{b}{d}\right)^{p} \qquad (2)$$

in which A is a constant, D is a diffusion parameter, k is Boltzmann's constant, T is absolute temperature, G is the shear modulus, b is the length of the Burgers vector, n is the stress exponent of the strain rate (=1/m, in which m denotes the strain-rate sensitivity of the flow stress), and p is the grain size exponent of the strain rate. For superplastic flow characterized by gbs accommodated by climb/glide of dislocations, n ~ 2 and p ~ 2. For gbs accommodated by diffusional flow, n ~ 1 and p ~ 2 or 3, depending on whether bulk (lattice) or boundary diffusion predominates.

The extension of the phenomenological relation between $\dot{\varepsilon}$, σ, T, and d expressed by Equation (2) to two- (or multi-) phase materials such as alpha/beta titanium alloys is not obvious. This is because an ambiguity arises as to which phase the values of D, G, Ω, d, and b relate and the relative strain and/or stress borne by each phase. For example, it is often assumed that d relates to the size of the alpha-phase particles and D to the diffusivity of solutes along the alpha-beta interfaces or within the beta phase; at other times an isostrain or isostress behavior of the two phases has been postulated [19-22].

The objective of the present work was to provide insight into the mechanisms of low-temperature superplasticity of alpha/beta titanium alloys, specifically the kinetics of coarsening during low-temperature processing and the effect of concurrent coarsening on plastic flow. To this end, a series of static heat treatments and isothermal compression tests were conducted using the same lot of ultrafine Ti-6Al-4V employed in two previous investigations of static and dynamic coarsening at high temperatures [14, 23]. In a companion paper [24], the tension behavior of a similar lot of ultrafine Ti-6Al-4V *sheet* material is reported.

II. MATERIAL AND PROCEDURES

A. *Material*

The present program utilized the same lot of ultra-fine microstructure Ti-6Al-4V used in the previous work on static and dynamic coarsening at high temperatures [14, 23]. The material comprised a billet measuring 150 mm diameter X 200 mm length fabricated at the Institute for Metals Superplasticity Problems (IMSP) (Ufa, Russia) [8]. It had a measured composition (in weight percent) of 6.3 aluminum, 4.1 vanadium, 0.18 iron, 0.18 oxygen, 0.010 carbon, 0.010 nitrogen, 0.002 hydrogen, balance titanium, and a beta-transus temperature T_β (at which alpha + beta $\rightarrow$ beta) of 995°C. The billet had been produced by beta annealing a preform at 1010°C for one hour followed by water quenching to produce a fine, Widmanstatten-alpha microstructure. The preform was then warm worked at 600°C via forging along three orthogonal directions to a cumulative von Mises effective strain of approximately 3. By this means, an

ultra-fine grain (UFG) microstructure of equiaxed alpha in a beta matrix was produced. The alpha-particle diameter was approximately 2.5 μm. Transmission electron microscopy (TEM) revealed that alpha-alpha sub-boundaries were also developed within the alpha particles, thus indicating an alpha grain/subgrain size of ~0.5 μm (Figure 1a). However, after relatively short annealing times (of the order of 15-30 minutes) at the warm-working temperatures of interest, almost all of the sub-boundaries appeared to have been eliminated, as indicated by the absence of channeling contrast in backscattered electron images (BSEI) taken in a scanning electron microscope (SEM) (Figures 1b, c). (Alpha-phase is the darker phase, and beta/transformed beta is the lighter phase in BSEI photographs of alpha-beta titanium alloys such as Ti-6Al-4V.) In addition, some of the alpha particles appeared to consist of remnants of alpha lamellae which had not fully globularized by the warm working operation. These ‘dog-leg’ shaped particles (e.g., those marked by arrows in Figure 1c) had internal alpha-alpha boundaries of very low misorientation as evidenced by their stability during long-term thermal exposure and deformation.

B. *Experimental Procedures*

1. Static Heat Treatments

Cylindrical samples measuring 12.5 diameter X 12.5 mm length were cut from the UFG Ti-6Al-4V billet and heat treated to establish the kinetics of coarsening at low processing temperatures. For this purpose, samples were enclosed in evacuated quartz capsules back filled with argon and heat treated at

650, 775 or 815°C for 0.25, 1, 4, 16, 64, or 96 hours. Each capsule was water quenched following heat treatment.

2. Isothermal Compression Tests

As in the previous effort [14], isothermal compression tests (and selected ring-compression tests) were conducted on the UFG Ti-6Al-4V program material to establish dynamic-coarsening kinetics and plastic-flow behavior at low processing temperatures, i.e., 650, 775, and 815°C.

The compression tests utilized cylindrical samples measuring 12.7 mm height X 8.46 mm diameter, which were compressed between silicon-nitride dies covered with boron-nitride-coated nickel foil. Following lubrication, the sample and tooling were induction heated to test temperature (using an iron-chromium-aluminum alloy susceptor) in approximately 10 minutes and soaked at temperature for an additional 15 or 60 minutes prior to compression in a 250 kN servo-hydraulic test system to an average axial (height) strain of 1.1[*]. Constant true strain rates of 10^{-4}, 10^{-3}, and 10^{-2} s^{-1} were used. Following compression, the ram, bottom die, and sample were lowered automatically and water quenched within 0.75 s of the completion of deformation.

To determine the strain-rate sensitivity of the flow stress as a function of strain and strain rate, selected additional isothermal, jump tests were conducted using cylindrical samples. These tests comprised imposing alternating strain rates of 10^{-4} and $3X10^{-4}$ s^{-1} or 10^{-3} and $3X10^{-3}$ s^{-1} at strain increments of ~0.1 to a total strain of 1.1.

[*] Compressive strains, strain rates, and stresses are reported as *positive* quantities here and throughout the balance of this paper.

Isothermal, compression tests were also conducted on *ring-shaped* samples of UFG Ti-6Al-4V to establish values of the friction shear factor for use in correcting flow stress data from the cylinder-compression tests. These samples had an OD, ID, height of 8.46 mm, 4.24 mm, and 2.82 mm, respectively; i.e., a 6:3:2 geometry. Ring tests were conducted at 775 and 815°C, a constant strain rate of 10^{-3} s^{-1}, and height reductions of approximately 30 and 55 percent.

3. Metallography

Extensive metallography was conducted following static heat treatment or compression testing to quantify coarsening behavior and the aspect ratio of each phase. Specifically, each sample was sectioned axially and prepared using standard metallographic techniques. A series of 2 to 4 BSEI photographs was then taken at the sample mid-height, mid-diameter location. Magnifications were chosen to ensure that ~100-800 total particles were sampled in the collection of micrographs for each test condition. The average alpha particle size, A_α, was determined by counting the number of particles, N_α, measuring the volume fraction of alpha, f_α, in each micrograph, and applying the relation $A_\alpha = f_\alpha A_T/N_\alpha$, in which A_T denotes the area of the micrograph. Those particles consisting of a 'dog-leg' geometry were counted as being 1.5 particles in number to provide an approximate estimate of the effect of their radii of curvature on coarsening behavior. The average alpha particle radius, $\bar{r}_\alpha$, was estimated from the value of A_α based on a circle with equivalent area. Because of the globular (non-spherical) nature of the particles, a stereological correction factor was not

utilized. The average alpha-particle radius ($\bar{r}_\alpha$) and beta-grain radius ($\bar{r}_\beta$) were also determined using a linear intercept technique. The two techniques showed excellent agreement. The overall uncertainty of the average particle/grain size measurements was estimated to be approximately $\pm$5 pct.

Additional, individual measurements of the geometry of alpha particles and beta grains were used to determine the aspect ratio of the phases before and after deformation.

4. Flow Curve Determination

Flow curves were determined from average pressure (p_{av}) - axial strain (ε) plots derived from the compression load-stroke data which were reduced assuming uniform deformation and corrected for the test-machine compliance. These curves were then further corrected for friction effects as in Reference 14 to obtain plots of true stress σ versus true strain ε.

III. RESULTS AND DISCUSSION

The principal results from this investigation related to static coarsening, dynamic coarsening, and the plastic-flow behavior of the UFG Ti-6Al-4V material. The findings in each area are summarized and discussed in the following sections.

A. *Static Coarsening*

1. Observations

Metallography on UFG Ti-6Al-4V samples heat treated at 650, 775, or 815°C for various times t revealed a measurable amount of coarsening of the

alpha particles (e.g., Figures 2 and 3 for 775 and 815°C, respectively). Not surprisingly, for a given heat-treatment time, the amount of coarsening increased with temperature. The micrographs also showed what appeared to be sporadic remnants of lamellae that had not been fully spheroidized in the as-received material (e.g., Figure 2c).

The coarsening rate and apparent coarsening mechanism were determined from plots of $\bar{r}_{\alpha}^{n} - \bar{r}_{\alpha o}^{n}$ versus $t - t_o$ (in which $\bar{r}_{\alpha o}$ $(t = t_o)$ denotes the average alpha particle radius at the initial time t_o) for values of the coarsening exponent n equal to 2 or 3. For times between 0 and 96 h, the results (e.g., Figures 4 and 5 for 775 and 815°C, respectively) indicated that the best straight-line fit corresponded to n =3 for all three test temperatures. A careful examination of the data for 775 and 815°C, however, suggested that the coarsening rate was slightly greater during early times, i.e., 0 to 4h. The value of n = 3 supports the conclusion that coarsening kinetics were controlled by diffusion of solutes through the beta phase. Summarized in Table I, values of the coarsening *rate* (slope K of r^3-vs-t plots) were considerably lower than previous measurements at higher temperatures [23], e.g., 6.0 μm^3/h at 900°C and 7.6 μm^3/h at 955°C.

The coarsening of the alpha particles was accompanied by a simultaneous increase in the beta grain size. In particular, a *Zener-like* relationship between the sizes of the alpha particles and beta grains was obtained when the alpha phase was treated as pinned grains and the beta grains as the pinning particles. Per the classical Zener model, the relationship between

the stable (limiting) *diameter* of the pinned phase (D_α) and the *radius* (r_β) and volume fraction (f_β) of the pinning particles is the following [25]:

$$D_\alpha = 4r_\beta/3f_\beta \qquad (3a)$$

or,

$$r_\alpha f_\beta / r_\beta = 2/3 \; . \qquad (3b)$$

For the 5 to 6 fold increase in alpha-particle and beta-grain sizes in the present work, the values of $r_\alpha f_\beta / r_\beta$ for 775 and 815°C fell in a relatively narrow range, i.e., ~0.35 to 0.50 (Table II), or a magnitude similar to 2/3. A similar trend was found upon analyzing previous static-coarsening data for 900 and 955°C [14, 23], also listed in Table II. (At 955°C, the major phase is beta, and thus the tabulated values are $r_\beta f_\alpha / r_\alpha$.) By contrast, the value of $r_\alpha f_\beta / r_\beta$ was ~0.2 at 650°C. However, the very large volume fraction of alpha and the difficulty in discerning individual alpha particles cast doubt on the reliability of the correlation at this temperature.

The present correlation of the alpha and beta sizes warrants further research, especially in view of the fact that the Zener relation is strictly applicable to microstructures with volume fractions of pinning particles equal to or less than 0.01. Nevertheless, it is of interest to note that observations for other alloys suggest a similar relationship. For instance, Senkov and Myshlyaev [26] noted that the ratio of the sizes of zinc-rich beta-phase grains and Al-rich alpha-phase grains (f_α = 0.45) in a Zn-22Al alloy remained approximately constant (≈1.15) during static annealing and during superplastic deformation. Although the degree of grain coarsening was much less (approximately two-fold) and occurred by a different mechanism (solute diffusion along grain boundaries) than in the present

work, the value of $r_\beta f_\alpha / r_\alpha$ in this prior effort (1.15 x 0.45 = 0.52) was very similar to that found here.

2. Interpretation of Static-Coarsening Rate

The kinetics of static coarsening were interpreted in the context of modified LSW (Lifshitz-Slyosov-Wagner) theory [25], as was employed in Reference 23. The original LSW theory is strictly applicable to the case of a matrix containing an infinitesimal volume fraction of second-phase particles of essentially pure solute. On the other hand, the modified LSW (MLSW) theory treats materials with a finite volume of particles whose composition is not necessarily a terminal solid solution. For a diffusion-controlled process, coarsening is described by the following relation:

$$\bar{r}_\alpha^3 - \bar{r}_{\alpha o}^3 = K_{MLSW}(t - t_o) \qquad (4)$$

in which

$$K_{MLSW} = \frac{8g(\phi)D\gamma_{\alpha\beta}C_\beta(1-C_\beta)V_M}{9RT(C_\alpha - C_\beta)^2[1+\partial \ln r / \partial \ln C_\beta]} \quad . \qquad (5)$$

In Equation (5) for the coarsening rate K_{MLSW}, $g(\phi)$ describes the functional dependence of the rate on the volume fraction of particles (ϕ); D denotes the diffusivity in the beta matrix of the rate limiting solute; $\gamma_{\alpha\beta}$ is the energy associated with particle-matrix (alpha-beta) interfaces (in J/m^2); C_β and C_α are the *equilibrium* concentrations in the beta matrix and alpha particle, respectively, of the rate-limiting solute (expressed as atomic fractions); V_M is the molar volume of the precipitate; R is the universal gas constant; T is the absolute temperature; and r is the activity coefficient of the rate-limiting solute in the beta matrix.

The present coarsening observations indicated that n = 3. Thus, low-temperature coarsening was likely limited by solute diffusion through the beta matrix. Because of uncertainties with respect to the function $g(\phi)$, the value of $K_{MLSW}/g(\phi)$ was estimated for each exposure temperature. For this purpose, the diffusivities of aluminum and vanadium in beta titanium, phase equilibria, and thermodynamic factors ($= 1 + \partial \ln r / \partial \ln C_\beta$) were taken from prior work [27, 28]. The molar volume of alpha particles, 10,440 mm^3, was determined from the mass of one mole of Ti-0.123Al-0.0185V (in atomic-fraction terms) (i.e., 45.4 g) and the density of the alpha phase (i.e., 4347 kg/m^3). As in previous work on coarsening at high temperatures [23], the value of $\gamma_{\alpha\beta}$ was taken to be equal to 0.4 J/m^2 because of the incoherent nature of alpha-beta interfaces.

Measured coarsening rates and predictions of $K_{MLSW}/g(\phi)$ are summarized and compared in Table III. Predictions based on vanadium diffusion are approximately equal to or lower than those for aluminum diffusion. Thus, it is likely that vanadium diffusion controlled the rate of coarsening. The comparison of listed measurements (for times between 0 and 4 h) and predictions based on vanadium diffusion suggests that $g(\phi)$ lies in the range of 4 to 8 for these temperatures (Table III). If the somewhat smaller K measurements for 0 to 96 hours (Table I) are used, $g(\phi)$ would be in the range of ~3 to 6. These values of $g(\phi)$ are comparable to those predicted by the simulations of Voorhees and Glicksman (i.e., g ~ 5.5) and the analysis of Brailsford and Wynblatt (i.e., g ~ 4.5) for the largest volume fraction each examined, i.e., $\phi = 0.7$ [29, 30]. This approximate agreement should be viewed as a qualitative result in light of the yet

larger volume fractions of second phase (~0.8 – 0.85) for the UFG Ti-6Al-4V at 650 - 815°C.

The comparison of measured and predicted coarsening rates could be affected if noticeable alpha-particle *coalescence* had occurred. Particle coalescence would lead to the formation of additional particles with grain or sub-boundaries. Quantitative analysis of a number of micrographs revealed that the number of boundaries, when scaled by the approximate amount of overall coarsening, did not increase, thus indicating that coalescence did not have a measurable effect on the static-coarsening rate. In addition, the distribution alpha-particle aspect ratios showed essentially no change during both static and dynamic coarsening, thus suggesting the absence of measurable coalescence.

B. *Dynamic Coarsening*

Substantial coarsening of the UFG Ti-6Al-4V also took place *during* deformation to a true strain of 1.1 at 775 and 815°C and strain rates of 10^{-4} and 10^{-3} s^{-1} (Figures 6 and 7). From a broad perspective, the amount of coarsening was greater for the higher test temperature and the longer-duration experiments (i.e., those at 10^{-4} s^{-1}). Furthermore, despite the difference in alpha-particle (and beta-grain) sizes after 15- versus 60-minute static preheats, the micrographs suggested that the final microstructures at a given temperature and strain rate were nearly the same. The quantitative measurements in Table II confirmed this observation. Thus, it was concluded that the dynamic coarsening rate was dependent on preheat time.

The dependence of the dynamic-coarsening rate on preheat time was quantified by calculating the values of K based on the alpha particle sizes at the beginning and end of deformation and assuming r^{3-} vs-t kinetics, as were found for dynamic coarsening at hot-working temperatures [14]. The results indicated that the dynamic-coarsening rate was indeed higher for the shorter preheat time for all combinations of strain rate and temperature (Table I). The effect was particularly noticeable for deformation at 10^{-3} s^{-1}.

Further examination of the measured coarsening rates (Table I) showed that the dynamic values were approximately 8 to 10 times greater than the static values. As for previous *high-temperature* observations, this increase can be attributed (at least partially) to enhanced diffusion associated with the generation of dislocation substructure in the beta phase through which solutes are being transported. The factor by which diffusion was enhanced during *low-temperature* deformation, however, was somewhat greater than that observed previously for high-temperature deformation, i.e., 4 to 6.

A plausible explanation for a number of the coarsening observations may be proposed based on the nature of the UFG Ti-6Al-4V material used in the present program. In particular, it is hypothesized that there is residual substructure in the beta phase due to the warm working operation used to manufacture the billet material. (Unfortunately, the decomposition of beta during cooling from high temperature makes it difficult to quantify such substructure.) At low heat-treatment temperatures, such substructure may not be eliminated during times of the order of several hours. Such a conclusion is supported by the

somewhat greater static-coarsening rates observed for “short” times (of the order of 0 to 4 hours) in comparison to those for “long” times (of the order of 0 to 96 hours). The effect of preheat time on the dynamic coarsening rate can be explained qualitatively in a similar manner. A short preheat time would leave more remnant substructure that would tend to lead subsequently to greater dynamic coarsening rates than that found for longer preheat times, as was observed. In addition, the preheat-time effect would be expected to be less for deformation at the slower strain rate (10^{-4} s^{-1}) because of the additional time available for the substructure to achieve an equilibrium condition.

C. *Plastic-Flow Behavior*

1. Flow Curves

True stress-true strain curves for the UFG Ti-6Al-4V material (Figures 8 and 9) revealed the influence of dynamic (and static) coarsening on plastic-flow behavior. Except for short transients at strains between 0 and ~0.2, the flow response at the lowest test temperature (650°C) and a strain rate of 10^{-3} s^{-1} (Figure 8a) showed almost steady-state flow except for the material tested after preheating for 15 minutes, which exhibited a small amount of flow hardening. Material preheated at the two longer times showed little flow hardening, albeit very similar (60-minute preheat) or slightly higher (4-h preheat) initial stresses compared to that for the 15-minute preheat. The absence of marked flow hardening can be ascribed to the minimal amount of dynamic coarsening that was measured. The slightly higher initial stress after the 4-h preheat was correlated with a small amount of static coarsening prior to deformation.

The plastic flow behavior at 775 and 815°C (Figures 8b, c) revealed that dynamic coarsening is mirrored by flow hardening, as was deduced earlier for high temperature flow [14]. However, the different preheat times in the present work provided important new insights (from scientific *and* industrial perspectives) on the interaction of static and dynamic coarsening. For deformation at 775°C and a strain rate of 10^{-4} s^{-1}, for example, marked flow hardening due to dynamic coarsening was found for preheat times of either 15 or 60 minutes (Figure 8b). For the 15-minute preheat time, the alpha particle and beta grain sizes almost quadrupled during deformation (Table II). The microstructural features increased in size during plastic flow following the 60-minute preheat as well, but only by a factor of 2.5, thus providing a plausible explanation for the lower flow-hardening rate for the longer preheat time. Moreover, the slightly higher initial stress for the 60-minute preheat was most likely due to the additional static coarsening prior to compression. The behavior at 775°C, 10^{-3} s^{-1} can be explained in a similar manner. The large amount of flow hardening after the 15-minute preheat mirrored the more than two-fold increase in particle/grain size, whereas the static coarsening interval of 60 minutes prior to deformation led to only a ~35-40 pct. increase in microstructural scale during deformation (Table II). These variations in coarsening led to almost the same final alpha particle size and beta grain size for the two preheat times (Table II) and thus, not surprisingly, almost identical flow stresses at the end of deformation (strain ~1.1). The flow behavior at 775°C and 10^{-2} s^{-1} can be explained on the basis of negligible dynamic coarsening and

the softening associated with high flow stresses and deformation heating at this strain rate [31].

The measured stress-strain response at 815°C (Figure 8c, Table II) was similar to that at 775°C. At 10^{-4} s^{-1}, the long duration of the deformation and concomitant dynamic coarsening overshadowed the effect on flow hardening of the difference in static coarsening characterizing the two different preheat times. On the other hand, the noticeable static coarsening during the longer preheat time led in turn to substantially less dynamic coarsening (and hence limited flow hardening) than the short preheat time for compression tests at 10^{-3} s^{-1}. The stress-strain curve for 10^{-2} s^{-1} suggested negligible dynamic coarsening and marked deformation heating.

The effect of preheat time on static and dynamic coarsening was also illustrated by comparing the previously-measured stress-strain curve at 900°C and 10^{-3} s^{-1} (using a 15 minute preheat) [14] and new results corresponding to a 60-minute preheat. The comparison (Figure 9) showed a noticeable effect of static coarsening on the initial flow stress. On the other hand, the flow hardening rates for the two preheat times were comparable, an effect that can be ascribed to the much more rapid rate of dynamic coarsening at the higher temperature (35 $\mu m^3/h$) compared to that at 775 and 815°C (~5-10 $\mu m^3/h$).

2. Strain-Rate Sensitivity

The strain-rate sensitivity of the flow stress (m value) as a function of strain for the UFG Ti-6Al-4V material at 650, 775, and 815°C (Figure 10) also provided insight into the nature of plastic flow. All of the measurements were

generally between 0.5 and 0.7, or values of m generally considered to be superplastic. For each test temperature, the m values were somewhat higher for a strain rate of 10^{-4} s^{-1} when compared to the results for 10^{-3} s^{-1}. Furthermore, the m's for 10^{-3} s^{-1} tended to decreased with strain. This effect was more noticeable for material that was preheated for 60 minutes. The present values of m were comparable to previous measurements at 900 and 950°C [14]. For example, m was ~0.7 for a strain rate of 10^{-3} s^{-1} at 900°C.

3. Interpretation of Flow Behavior

The low-temperature plastic flow of the UFG Ti-6Al-4V billet material exhibited the signature of superplasticity, i.e., high m values and the retention of a relatively equiaxed shape of the phases after large deformation. Furthermore, no significant crystallographic texture was observed in the as-received or deformed samples. In addition, the m values and alpha-particle coarsening behavior found for the billet material were similar to observations for low-temperature deformation of a similar UFG Ti-6Al-4V *sheet* material which exhibited elongations in excess of 700 pct. [24]. Thus, it may be concluded that the majority of the imposed deformation was accommodated by relative sliding between the alpha and beta phases, referred to here simply as grain boundary sliding (gbs).

It is unlikely that an isostrain model of the deformation of two-phase microstructures [21] which excludes gbs can explain the stress-strain response of the UFG Ti-6Al-4V at low temperatures. In the absence of gbs, isostrain models based on the behavior of the discrete alpha and beta phases (such as shown in

Figure 11) would likely lead to overall flow stresses at the test temperatures of interest here that are an order of magnitude greater than those measured. Even if the bulk of the imposed strain is borne by gbs, stress concentrations generated at interphase triple points would have to be accommodated by some degree of intragranular slip. Based on the flow stress of the individual phases, such intragranular slip would likely be accommodated in the beta phase, possibly near the interface where strain concentration is more likely, rather than equally by the alpha and beta phases. Similar remarks would also apply to self-consistent models for two-phase structures [34, 35] inasmuch as such approaches tend to weight the overall behavior in favor of the phase with the larger volume fraction (i.e., the alpha phase in the present work).

The interpretation of the low-temperature superplastic flow behavior thus reduces to determining the mechanism by which gbs is accommodated, e.g., by slip within the beta phase or diffusion within the beta or along alpha-beta boundaries. To develop a first-order understanding, the flow stress data were therefore interpreted in the context of Equation (2)[†] and a core-mantle type hypothesis for which the grain/core size (d) was taken to be the alpha particle size (d_α) and the other parameters were based on the properties of the mantle-like beta regions surrounding the alpha particles.

Values of m between ~0.5 and 0.7 suggested that the stress exponent n was between ~1.4 and 2. Such stress exponents indicate that gbs was likely

[†] A term comprising the volume fraction of beta was not included in Equation (2) as in Reference 22 because it was hypothesized that the deformation of beta, which accommodates gbs, is local in nature and analogous to mantle deformation in the description of superplasticity of single-phase alloys formulated by Gifkins [15].

accommodated to various degrees by dislocation glide-climb (which would yield n = 2, as in the core-mantle model of Gifkins [15]) as well as by diffusional processes (for which n = 1). Furthermore, the grain-size exponent of the strain rate (p) was found to be between ~1.6 and ~2.2 by applying the relation $p = n\,[\log(\sigma_2/\sigma_1)]\,/[\log(r_{\alpha_1}/r_{\alpha_2})]$, in which the flow stresses (σ) and grain sizes (r_α) were evaluated at the beginning and end of each compression test. The value of p = 2 also corresponds to gbs accommodated by dislocation processes or lattice (bulk) diffusion.

The value of G in Equation (2) was taken to be the shear modulus of beta titanium (G ~ 20 GPa [36]); the temperature dependence of G was neglected based on ultrasonic measurements of Young's modulus which indicated little effect for the range of 750 to 950°C [37]. Similarly, the burgers vector b was assumed to be that for unalloyed beta titanium (0.287 nm). The measured alpha particle size diameter d_α was taken to be the appropriate microstructural parameter for d.

The efficacy of Equation (2) in representing the flow behavior of the ultrafine Ti-6Al-4V was ascertained by re-arranging it to obtain an expression for the product of the two unknown quantities, AD, viz.,

$$AD = \left(\frac{\dot{\varepsilon} kT}{Gb}\right)\left(\frac{G}{\sigma}\right)^n \left(\frac{d}{b}\right)^p \qquad (6)$$

Values of the right-hand side of Equation (6) were calculated using measurements of σ and d_α for compression experiments at strain rates of 10^{-3} and 10^{-4} s^{-1} from the present work at low temperatures using preheat times of

0.25 and 1 h and previous results [14] from high temperatures (900, 955°C), assuming p = 2 and n = 1.67 (= 1/0.6, where 0.6 ~ the average m value in the superplastic regime). A semi-log plot of this quantity as a function of inverse temperature (Figure 12a) was compared to two similar graphs: (a) one in which the beta grain diameter (d_β) was taken to be the pertinent microstructural parameter d in Equation (6) and (b) the other using d = d_α *calculated* from the expression $d_\alpha = 0.45 \times d_\beta/f_\beta$ per the results in Table II. Each of the results in Figure 12a shows a linear behavior from which an apparent activation energy Q for the diffusivity D was obtained. These values were 160 kJ/mol for the plot based on d_α and 284 kJ/mol for the one based on d_β. Furthermore, the plot based on the measured values of d_α and those calculated from d_β show excellent agreement, underscoring the relation between the alpha particle size and beta grain size. Although the plot for d = d_α is probably more realistic than that for d = d_β based on a core-mantle interpretation of superplastic flow, the anomalously large activation energy for the d = d_β plot can be rationalized as an artifact associated with the variation of the beta volume fraction with temperature.

A physical interpretation of the activation energies so determined was obtained by comparison with published data for vanadium and aluminum solute diffusion and self diffusion in beta titanium (Figure 12b). The value of Q based on d = d_α (160 kJ/mol) is close to those determined for the bulk diffusivity of vanadium and aluminum in beta titanium (145 and 150 kJ/mole, respectively) [27] and for self diffusion in beta titanium (131-153 kJ/mole) [38-40] at temperatures between 900 and 1540°C. These values of Q are lower than those previously

determined for Ti-6Al-4V in the superplastic domain (i.e., 176 - 330 kJ/mole) [10, 19, 20, 41]. In previous work, however, the effect of alpha particle or beta grain growth on the flow stress was not considered as carefully as in the present work.

A comparison of the plot of AD vs 1/T (for $d = d_\alpha$) and that for D vs 1/T for solute/self diffusion in an annealed beta titanium matrix (Figure 12b) provides an estimate of A or the factor needed to account for the enhancement of diffusion due to concurrent deformation. This comparison suggests that A ~10, or a value similar in magnitude to that which quantifies the relationship between static and dynamic coarsening.

Comparison of the present and previous efforts [10] also reveals the importance of the alpha particle size, rather than the size of alpha grains within each particle, in controlling superplastic flow of SPD alpha/beta titanium alloys. The material in the previous work had a fine alpha grain size and coarse alpha particle size and hence exhibited modest m values (~0.35) and tensile ductility. This is as expected in view of the relative ease of sliding at alpha/beta boundaries compared to that at alpha/alpha boundaries [42].

IV. SUMMARY AND CONCLUSIONS

The low-temperature static- and dynamic-coarsening kinetics and plastic-flow behavior of Ti-6Al-4V with an ultra-fine grain (UFG) microstructure were established via a series heat treatments and isothermal compression tests. From this work, the following conclusions were drawn:

1. UFG Ti-6Al-4V undergoes measurable static coarsening over periods of time of the order of 0 to 100 h. This coarsening follows r^3- vs - time kinetics and is

thus diffusion controlled. Slightly higher coarsening rates for short times of the order of 0 to 4 h (compared to those for longer times) suggest that a certain degree of warm work is retained after the SPD process used to make the UFG material. The effect of volume fraction on the static-coarsening rate at low temperatures is similar to that previously observed at high temperatures ($\geq 900^{o}C$).

2. Dynamic coarsening at low temperatures ($<900^{o}C$) occurs at rates which are approximately one order of magnitude faster than the corresponding static-coarsening rates, much like at higher temperatures. This behavior can be ascribed to the enhancement of diffusion by concurrent deformation.
3. Dynamic coarsening at low temperatures gives rise to noticeable flow hardening.
4. The deformation behavior of UFG Ti-6Al-4V at low temperatures and strain rates of the order of 10^{-4} and 10^{-3} s^{-1} is superplastic with m values of ~0.6. Interphase sliding, which characterizes superplastic deformation, is accommodated by both dislocation glide-climb and bulk-diffusion processes.
5. Deformation (and diffusion) within the softer beta phase (and near its interface with alpha-phase particles) appears to control the constitutive response of UFG Ti-6Al-4V. With this assumption, an approximate description of the interdependence of stress, strain rate, and grain/particle size is obtained. For the two-phase Ti-6Al-4V alloy, the alpha particles and beta grains appear to play roles similar to the core and mantle, respectively, in

classical models of superplasticity developed originally for single-phase materials.

Acknowledgements – This work was conducted as part of the in-house research of the Metals Processing Group of the Air Force Research Laboratory's Materials and Manufacturing Directorate. The support and encouragement of the laboratory management and the Air Force Office of Scientific Research (Dr. B. Conner, program manager) are gratefully acknowledged. One of the authors (GAS) thanks the University of Dayton for granting a period of sabbatical leave during which this work was done. Technical discussions with Prof. G.A. Salishchev (Institute for Metals Superplasticity Problems, Ufa, Russia), who also supplied the material, Prof. C.S. Lee (Pohang University of Science and Technology, Pohang, Korea), and Dr. Oleg Senkov (UES, Inc., Dayton, OH) are also gratefully acknowledged.

References

1. Y.T. Zhu, T.G. Langdon, R.Z. Valiev, S.L. Semiatin, D.H. Shin, and T.C. Lowe: *Ultrafine Grained Materials III*, TMS, Warrendale, PA, 2004
2. Y.T. Zhu, T.G. Langdon, Z. Horita, M.J. Zehetbauer, S.L. Semiatin, and T.C. Lowe, eds.: *Ultrafine Grained Materials IV*, TMS, Warrendale, PA, 2006.
3. M.J. Zehetbauer and R.Z. Valiev, eds.: *Proc. Second International Conference on Nanomaterials by Severe Plastic Deformation: Fundamentals-Processing-Applications*, Wiley-VCH, Weinheim, Germany, 2004.
4. E. Ma: *JOM*, April 2006, vol. 58, no. 4, pp. 49-53.
5. P. Comley: *Mat. Sci. Forum*, 2004, vols. 447-448, pp. 233-238.
6. P. Comley: *J. Mater. Eng. Perf.*, 2004, vol. 13, pp. 660-664.
7. H. Inagaki: *Z. fur Metallkunde*, 1995, vol. 86, pp. 643-650.
8. S.V. Zherebstov, G.A. Salishchev, R.M. Galeyev, O.R. Valiakhmetov, and S.L. Semiatin: *Proc. Second International Conference on Nanomaterials by*

Severe Plastic Deformation: Fundamentals-Processing-Applications, M.J. Zehetbauer and R.Z. Valiev, eds., Wiley-VCH, Weinheim, Germany, 2004, pp. 835-840.

9. G.A. Salishchev, R.M. Galeyev, O.R. Valiakhmetov, R.V. Safiullin, R.Y. Lutfullin, O.N. Senkov, F.H. Froes, and O.A. Kaibyshcv: *J. Mater. Proc. Techn.*, 2001, vol. 116, pp. 265-68.
10. Y.G. Ko, C.S. Lee, D.H. Shin, and S.L. Semiatin: *Metall. and Mater. Trans. A*, 2006, vol. 37A, pp. 381-391.
11. A.K. Ghosh: Unpublished research, University of Michigan, Ann Arbor, MI, 2006.
12. A.V. Sergueeva, V.V. Stolyarov, R.Z. Valiev and A.K. Mukherjee: *Mater. Sci. Eng. A,* 2002, vol. A323, pp. 318-25.
13. A.K. Ghosh and C.H. Hamilton: *Metall. Trans. A*, 1979, vol. 10A, pp. 699-706.
14. S.L. Semiatin, M.W. Corbett, P.N. Fagin, G.A. Salishchev, and C.S. Lee: *Metall. and Mater. Trans. A*, 2006, vol. 37A, pp. 1125-1136.
15. R.C. Gifkins: *Metall. Trans. A*, 1976, vol. 7A, pp. 1225-1232.
16. A.K. Ghosh in: *Metalworking: Bulk Forming*, Volume 14A, ASM Handbook, Tenth Edition, S.L. Semiatin, ed., ASM International, Materials Park, OH, 2005, pp. 563-586.
17. J.E. Bird, A.K. Mukherjee, and J. E. Dorn in: *Quantitative Relation Between Microstructure and Properties*, D.G. Brandon and A. Rosen, eds., Israel Universities Press, Jerusalem, Israel, 1969, pp. 255-342.

18. T.G. Langdon: J. Mater. Sci., 2006, vol. 41, pp. 597-609.
19. M.L. Meier, D.R. Lesuer, and A.K. Mukherjee: *Mater. Sci. and Eng. A*, 1991, vol. A136, pp. 71-78.
20. A. Arieli and A. Rosen, *Metall. Trans. A*, 1977, vol. 8A, pp. 1591-1596.
21. J.A. Wert and N.E. Paton: *Metall. Trans. A*, 1983, vol. 14A, pp. 2535-2544.
22. M. Tufts and C. Hammond: *Mater. Sci. and Techn.*, 1999, vol. 15, pp. 1154-1166.
23. S.L. Semiatin, B.C. Kirby, and G.A. Salishchev: *Metall. Mater. Trans. A*, 2004, vol. 35A, pp. 2809-2819.
24. G.A. Sargent and S.L. Semiatin: Unpublished research, Air Force Research Laboratory, Wright-Patterson Air Force base, OH, 2006.
25. J.W. Martin, R.D. Doherty, and B. Cantor: *Stability of Microstructure in Metallic Systems*, Cambridge University Press, Cambridge, UK, 1997.
26. O. N. Senkov and M.M. Myshlyaev: *Acta Metall.*, 1986, vol. 34, pp. 97-106.
27. S.L. Semiatin, T.M. Brown, T.A. Goff, P.N. Fagin, D.R. Barker, R.E. Turner, J.M. Murry, J.D. Miller, and F. Zhang: *Metall. Mater. Trans. A*, 2004, vol. 35A, pp. 3015-3018.
28. S.L. Semiatin, S.L. Knisley, P.N. Fagin, F. Zhang, and D.R. Barker: *Metall. Mater. Trans. A*, 2003, vol. 34, pp. 2377-2386.
29. P.W. Voorhees and M.E. Glicksman: *Acta Metall.*, 1984, vol. 32, pp. 2013-2030.
30. A.D. Brailsford and P. Wynblatt: *Acta Metall.*, 1979, vol. 27, pp. 489-497.

31. R.L. Goetz and S.L. Semiatin: *J. Mater. Eng'g. Perf.*, 2001, vol. 10, pp. 710-717.

32. J.D. Miller, G.A. Sargent and S.L. Semiatin: Unpublished research, Air Force Research Laboratory, Wright-Patterson Air Force base, OH, 2006.

33. G. Schroder and T.W. Duerig in: *Titanium: Science and Technology*, G. Lutjering, U. Zwicker, and W. Bunk, eds., Deutsche Gesellschaft fur Metallkunde e.V., Oberursel, Germany, 1985, pp. 585-592.

34. S.L. Semiatin, F. Montheillet, G. Shen, and J.J. Jonas: *Metall. Mater. Trans. A*, 2002, vol. 33A, pp. 2719-2727.

35. P. Vo, M. Jahazi, S. Yue, and P. Bocher: *Mater. Sci. and Eng.* A, 2007, vol. A447, pp. 99-110.

36. H. Ogi, S. Kai, H. Ledbetter, R. Tarumi, M. Hirao, and K. Takashima: *Acta Mater.*, 2004, vol. 52, pp. 2075-2080.

37. S.M Goodrich: Unpublished research, University of Dayton Research Institute, Dayton, OH, 2006.

38. J. F. Murdock, T. S. Lundy and E. E. Standsbury, *Acta Metall.*, 1964, vol. 12, 1033-1039.

39. J. F. Murdock, and C. J. McHargue, *Acta Metall.*, 1968, vol. 16, 493-500

40. N. E. W. De Reca and C. M. Libanati, *Acta Metall.*, 1968, vol 16, 1297-1305

41. T. Seshacharyulu, S.C. Medeiros, W.G. Frazier, and Y.V.R.K. Prasad: *Mater. Sci. and Eng. A*, 2000, vol. A284, pp. 184-194.

42. J.H. Kim, S.L. Semiatin, and C.S. Lee: *Mate Sci and Eng A*, 2005, vol. A394, pp. 366-375.

Table I. Measured Values of the Coarsening Rate K ($\mu m^3/h$) of Alpha Particles in UFG Ti-6Al-4V Billet Material

Temperature (C)	Static (0-4 h)*	Static (0-96h)**	Dynamic†: 10^{-4} s^{-1}		Dynamic†: 10^{-3} s^{-1}	
			0.25 h	1 h	0.25 h	1 h
650	0.025	0.025	---	---	---	---
775	0.66	0.48	5.16	3.25	7.41	5.14
815	0.83	0.68	4.86	4.35	12.1	3.87

* Based on alpha particle radii ($\bar{r}_\alpha$) at t = 0 and t = 4 h

** Based on best fit straight line of all $\bar{r}_\alpha^3 - \bar{r}_{\alpha o}^3$ vs time data (0 – 96 h)

† Dynamic coarsening values are for sample preheat times of 0.25 or 1 h

Table II. Measured Sizes of Alpha Particles and Beta Grains in UFG Ti-6Al-4V

Temp (°C)	Strain	Preheat Time (h)	Strain Rate (s^{-1})	r_α (μm)	r_β (μm)	f_β (pct.)	r_α/r_β	$r_\alpha f_\beta/r_\beta$
650	0	.25	--	0.36	0.099	4.2	3.60	0.15
	0	1	--	0.46	0.126	5.6	3.65	0.20
	0	4	--	0.52	0.152	5.6	3.42	0.19
	0	16	--	0.70	0.202	5.8	3.46	0.20
	0	48	--	1.09	0.310	5.2	3.52	0.18
	0	96	--	1.33	0.386	6.1	3.45	0.21
	1.1	.25	0.001	0.59	0.153	4.7	3.86	0.18
	1.1	1	0.001	0.62	0.148	5.0	4.19	0.21
775	0	0.25	--	0.632	0.214	14	2.95	0.41
	0	1	--	1	0.34	12	2.94	0.35
	0	4	--	1.4	0.51	14	2.75	0.39
	0	16	--	1.88	0.697	14	2.7	0.38
	0	96	--	3.59	1.2	14	2.99	0.42
	1.1	0.25	0.001	1.36	0.484	14	2.81	0.39
	1.1	0.25	0.0001	2.52	0.753	14	3.35	0.47
	1.1	1	0.001	1.37	0.48	13	2.85	0.37
	1.1	1	0.0001	2.22	0.783	14	2.84	0.40
815	0	0.25	--	0.739	0.298	19	2.48	0.47
	0	0.5	--	0.79	0.374	19	2.11	0.40
	0	1	--	1.07	0.47	18	2.28	0.41
	0	4	--	1.52	0.698	18	2.18	0.39
	0	16	--	2.19	0.914	18	2.4	0.43
	0	96	--	4.04	1.74	19	2.32	0.44
	1.1	0.25	0.001	1.6	0.653	19	2.45	0.47
	1.1	0.25	0.0001	2.48	1.05	20	2.36	0.47
	1.1	1	0.001	1.34	0.54	16	2.48	0.40
	1	1	0.0001	2.44	1.02	18	2.39	0.43
900	0	0.5	0	0.96	0.813	45	1.18	0.53
	0.5	0.25	0.0001	2.13	1.78	44	1.2	0.53
	1.4	0.25	0.0001	3.19	2.12	35	1.5	0.52
	1.4	0.25	0.001	2.40				
	1.1	1	0.001	1.78	1.58	44	1.13	0.50
								$r_\beta f_\alpha/r_\alpha$
955	0	0.5	0	1.15	1.67	76	0.69	0.35
	0.5	0.25	0.0001	2.9	4.45	74	0.65	0.40
	1.4	0.25	0.0001	3.6	5.04	64	0.87	0.50
	1.4	0.25	0.001	3.30				
	1.1	1	0.001	2.60	4.15	61	0.63	0.38

Table III. Comparison of Measured* and Predicted** Static-Coarsening Rates

Temp (°C)	v/o Alpha	Solute	Comp Term†	Meas. K ($\mu m^3/h$)	K_{MLSW} ($\mu m^3/h$) ($\gamma_{\alpha\beta}$ = 0.4 J/m^2)	Ratio
650	0.94	Al	9.25	0.025	0.0054	---
650	0.94	V	6.78	0.025	0.0056	4.5
775	0.88	Al	21.4	0.66	0.107	---
775	0.88	V	11.8	0.66	0.0796	8.3
815	0.82	Al	29.7	0.83	0.278	---
815	0.82	V	15.6	0.83	0.191	4.3

* Measurements for 0 – 4 h

** Predictions assuming $g(\phi) = 1$

† Composition term $\equiv C_\beta(1 - C_\beta)/(C_\alpha - C_\beta)^2$

Figure Captions

Figure 1. Microstructure of UFG Ti-6Al-4V billet produced by IMSP: (a) TEM micrograph of as-received material and SEM micrographs of material water quenched after a 15-minute heat treatment at (b) 775°C or (c) 815°C.

Figure 2. Backscattered electron images of the microstructure developed in UFG Ti-6Al-4V during heat treatment at 775°C for times of (a) 0.25, (b) 1, (c) 4, or (d) 16 hours. All of the micrographs were shot at the same magnification.

Figure 3. Backscattered electron images of the microstructure developed in UFG Ti-6Al-4V during heat treatment at 815°C for times of (a) 0.25, (b) 1, (c) 4, or (d) 16 hours. All of the micrographs were shot at the same magnification.

Figure 4. Plots of $\bar{r}_{\alpha}^{n} - \bar{r}_{\alpha o}^{n}$ versus $t - t_o$ for heat treatments of UFG Ti-6Al-4V at 775°C and values of n equal to (a) 2 or (b) 3.

Figure 5. Plots of $\bar{r}_{\alpha}^{n} - \bar{r}_{\alpha o}^{n}$ versus $t - t_o$ for heat treatments of UFG Ti-6Al-4V at 815°C and values of n equal to (a) 2 or (b) 3.

Figure 6. Backscattered electron images of microstructures developed in UFG Ti-6Al-4V at 775°C during (a, b) static heat treatment or (c-f) deformation to a true axial strain of 1.1 following preheating. The soak/preheat time was (a, c, e) 15 min. or (b, d, f) 60 min., and the

imposed strain rate was (c, d) 10^{-4} s^{-1} or (e, f) 10^{-3} s^{-1}. The compression axis is vertical in all micrographs.

Figure 7. Backscattered electron images of microstructures developed in UFG Ti-6Al-4V at 815°C during (a, b) static heat treatment or (c-f) deformation to a true axial strain of 1.1 following preheating. The soak/preheat time was (a, c, e) 15 min. or (b, d, f) 60 min., and the imposed strain rate was (c, d) 10^{-4} s^{-1} or (e, f) 10^{-3} s^{-1}. The compression axis is vertical in all micrographs.

Figure 8. Friction-corrected flow curves for UFG Ti-6Al-4V preheated for 15 or 60 minutes and deformed at strain rates of 10^{-4}, 10^{-3}, or 10^{-2} s^{-1} at (a) 650°C, (b) 775°C, or (c) 815°C.

Figure 9. Friction-corrected flow curves for UFG Ti-6Al-4V preheated for 15 or 60 minutes and deformed at strain rates of 10^{-4}, 10^{-3}, or 10^{-2} s^{-1} at 900°C.

Figure 10. Strain-rate sensitivity measurements for UFG Ti-6Al-4V from jump tests at (a) 650°C, (b) 775°C, or (c) 815°C.

Figure 11. Flow stress data for (a) the single-phase alpha alloy Ti-7Al-1.5V with a grain size of ~75 μm [32] and (b) the beta titanium alloy Ti-10V-2Fe-3Al with a grain size of ~10 μm [33].

Figure 12. Semilog plots used to determine the deformation mechanism during superplastic flow of ultrafine Ti-6Al-4V: (a) AD vs 1/T using $d = d_\alpha$ or d

= d_β and (b) a comparison of AD measurements with literature data for solute and self diffusion in beta titanium.

35

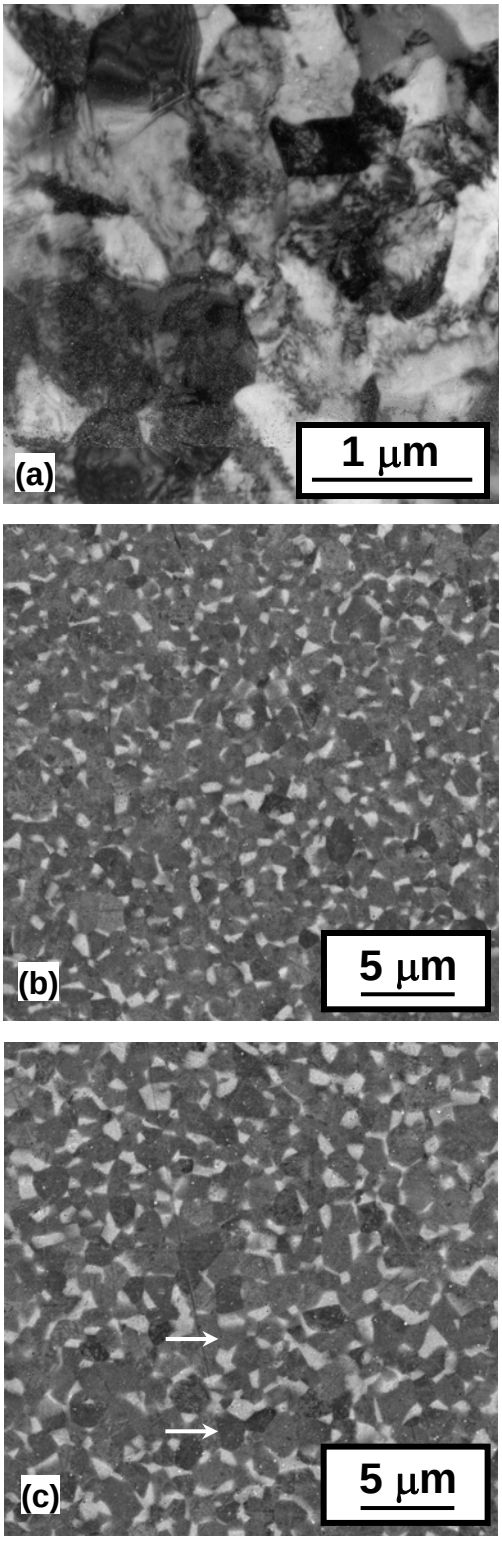

Figure 1. Microstructure of UFG Ti-6Al-4V billet produced by IMSP: (a) TEM micrograph of as-received material and SEM micrographs of material water quenched after a 15-minute heat treatment at (b) 775°C or (c) 815°C.

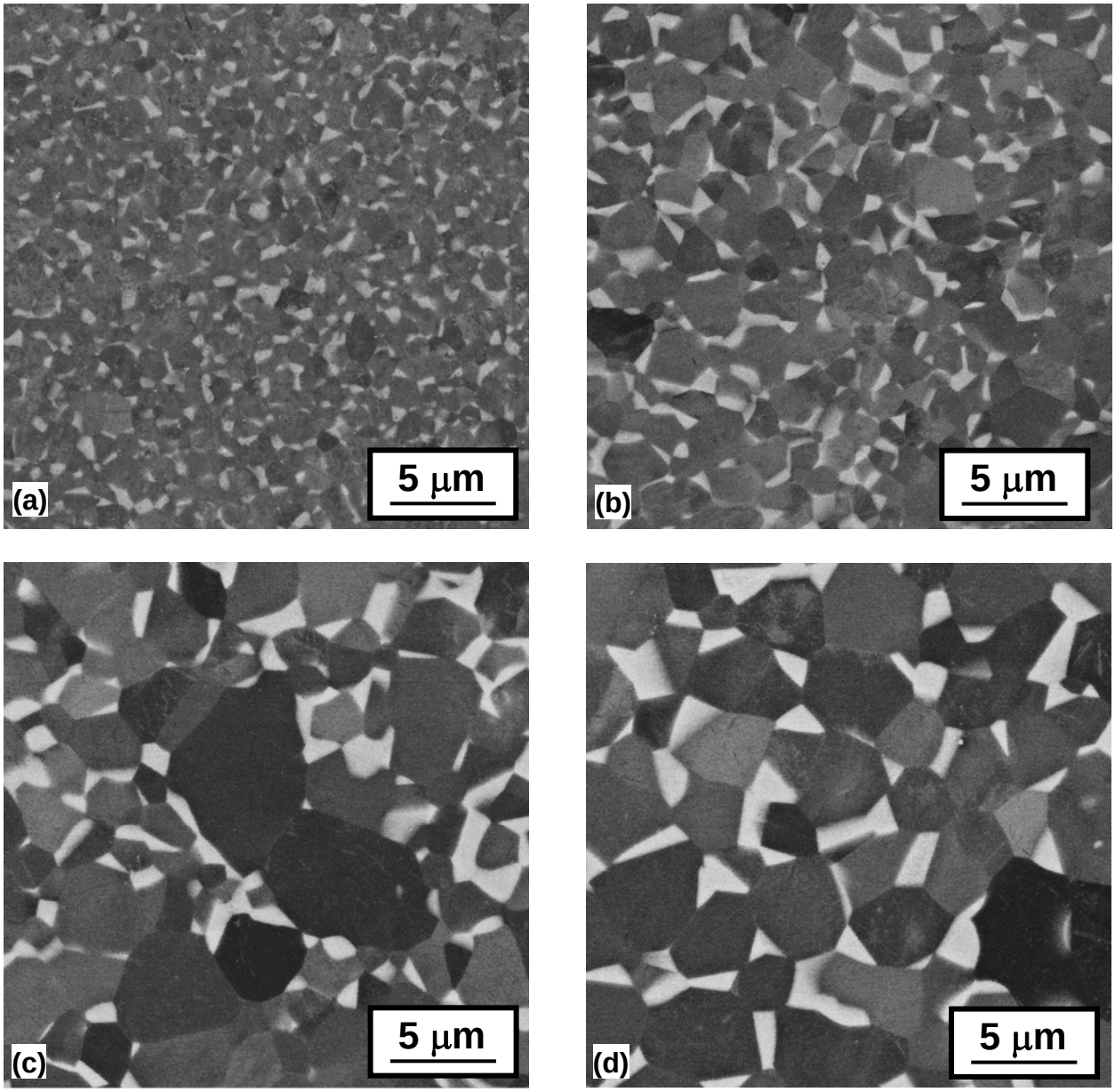

Figure 2. Backscattered electron images of the microstructure developed in UFG Ti-6Al-4V during heat treatment at 775°C for times of (a) 0.25, (b) 1, (c) 4, or (d) 16 hours. All of the micrographs were shot at the same magnification.

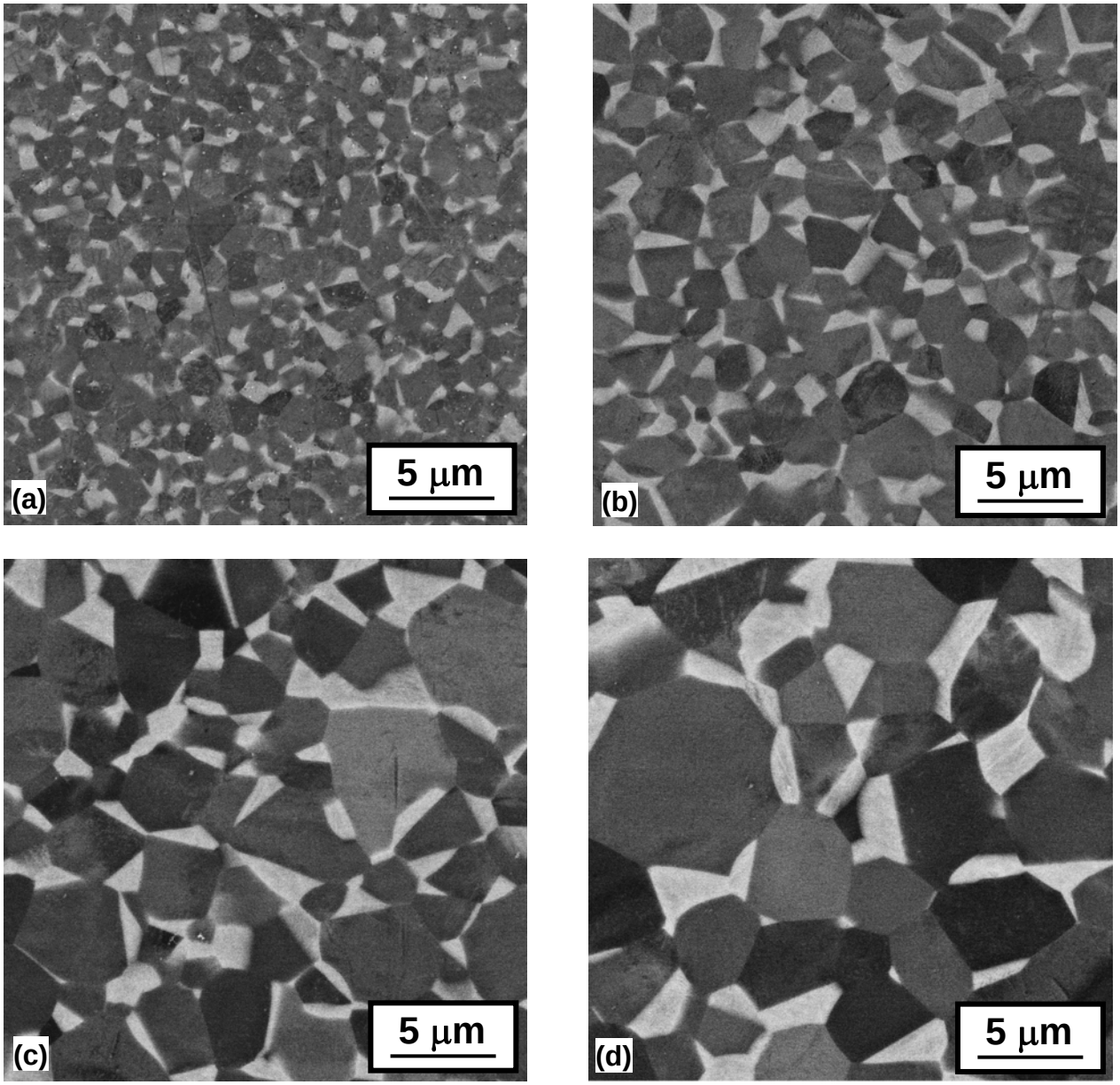

Figure 3. Backscattered electron images of the microstructure developed in UFG Ti-6Al-4V during heat treatment at 815°C for times of (a) 0.25, (b) 1, (c) 4, or (d) 16 hours. All of the micrographs were shot at the same magnification.

(a)

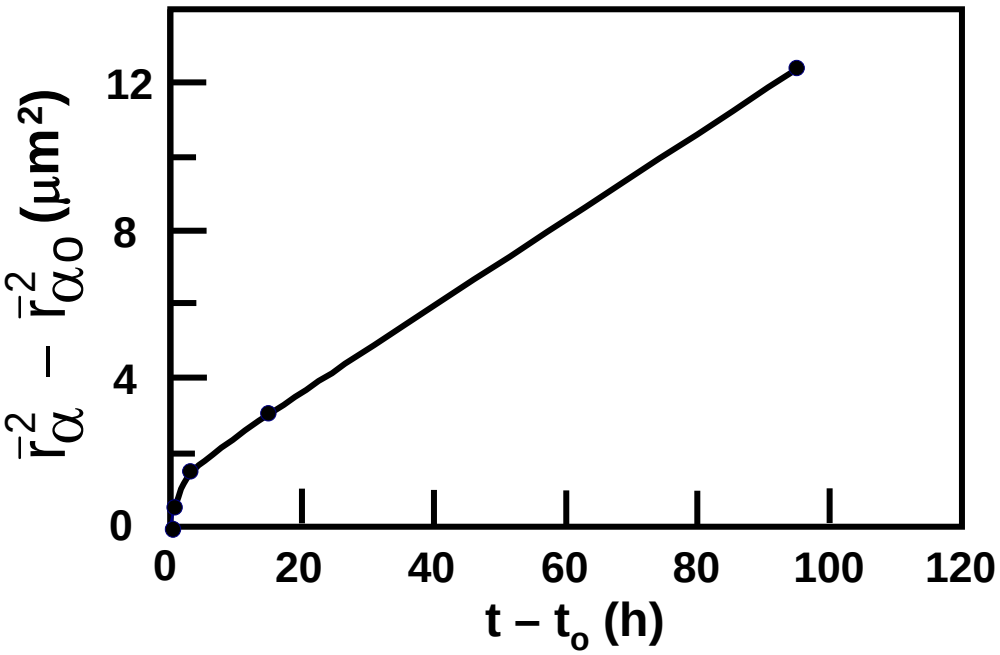

(b)

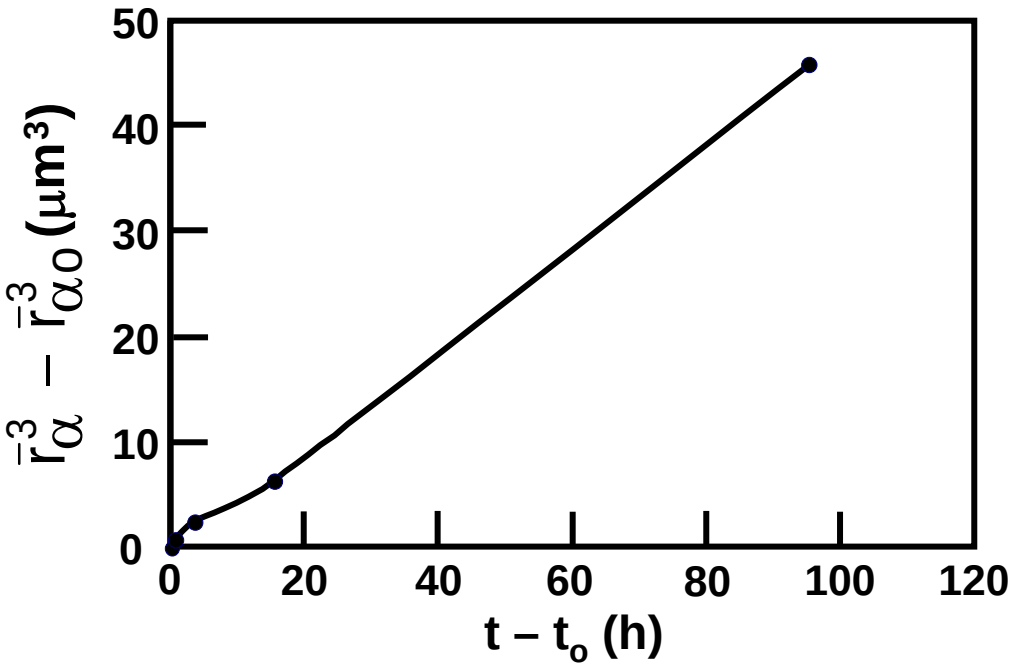

Figure 4. Plots of $\bar{r}_\alpha^n - \bar{r}_{\alpha o}^n$ versus $t - t_o$ for heat treatments of UFG Ti-6Al-4V at 775°C and values of n equal to (a) 2 or (b) 3.

(a)

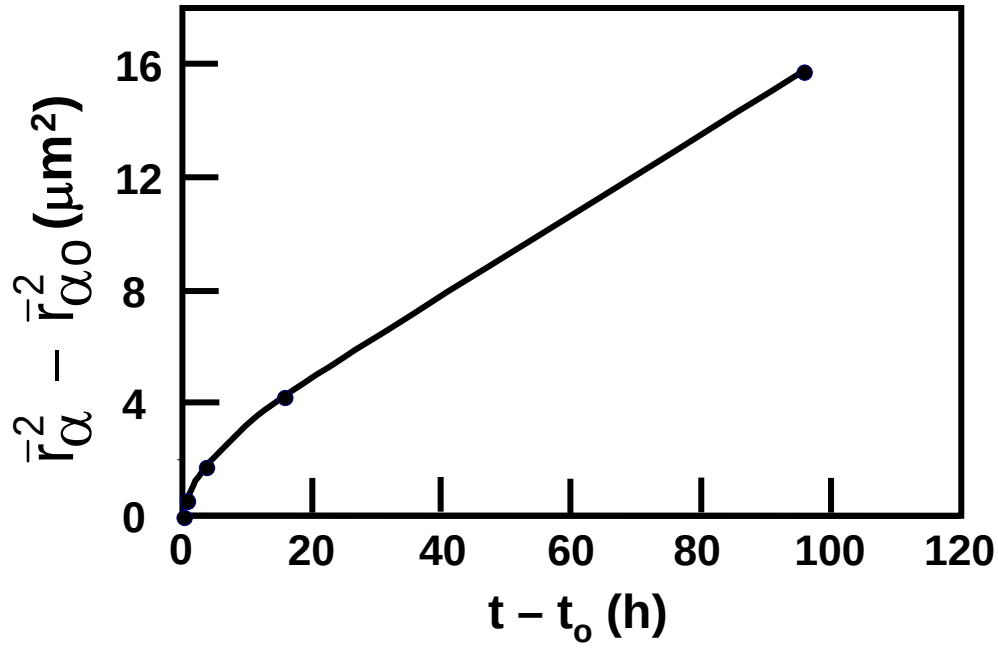

(b)

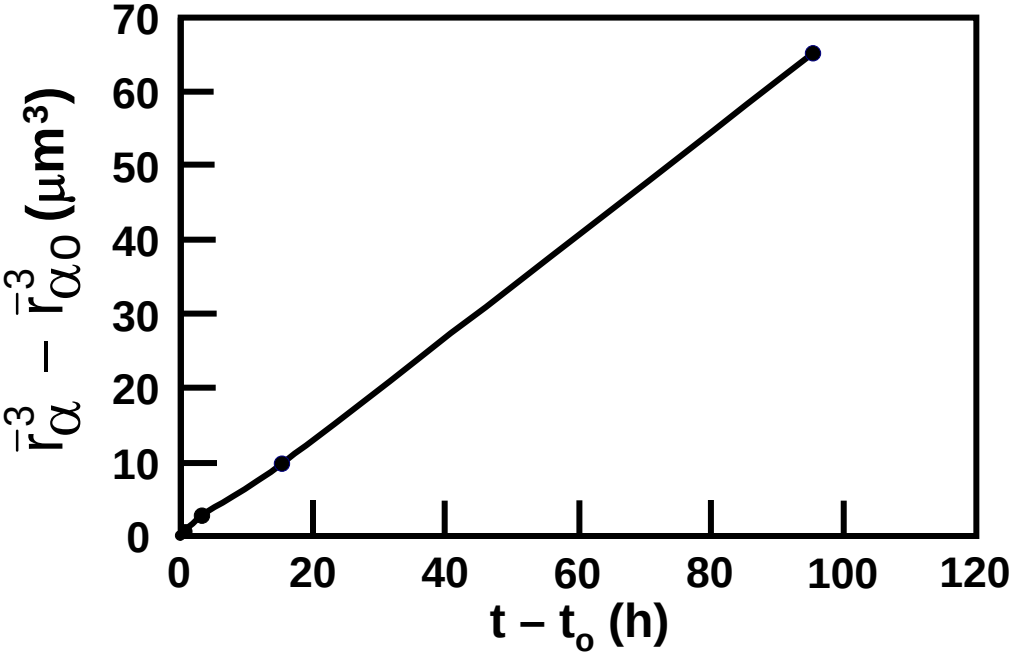

Figure 5. Plots of $\bar{r}_\alpha^n - \bar{r}_{\alpha o}^n$ versus $t - t_o$ for heat treatments of UFG Ti-6Al-4V at 815°C and values of n equal to (a) 2 or (b) 3.

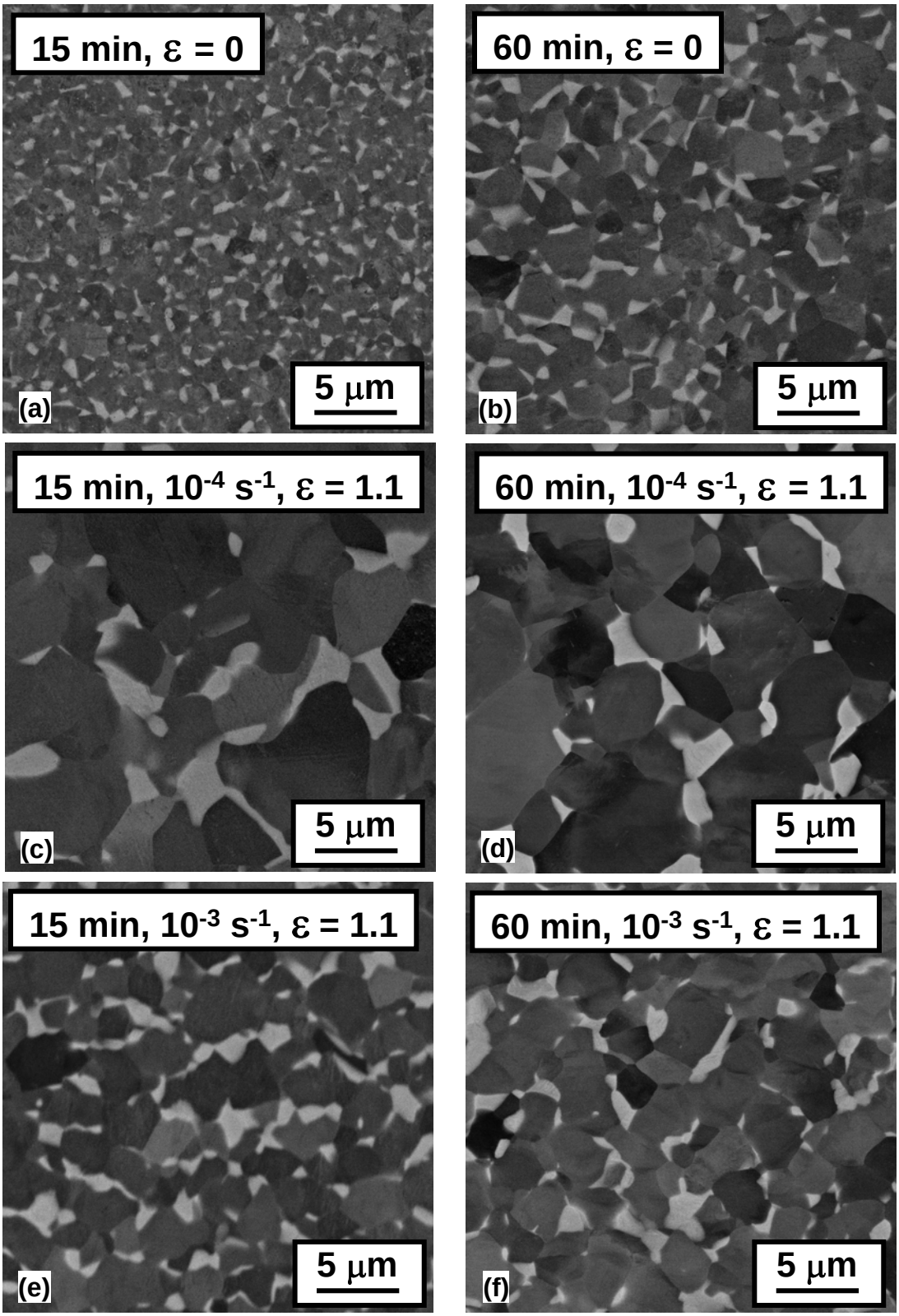

Figure 6. Backscattered electron images of microstructures developed in UFG Ti-6Al-4V at 775°C during (a, b) static heat treatment or (c-f) deformation to a true axial strain of 1.1 following preheating. The soak/preheat time was (a, c, e) 15 min. or (b, d, f) 60 min., and the imposed strain rate was (c, d) 10^{-4} s^{-1} or (e, f) 10^{-3} s^{-1}. The compression axis is vertical in all micrographs.

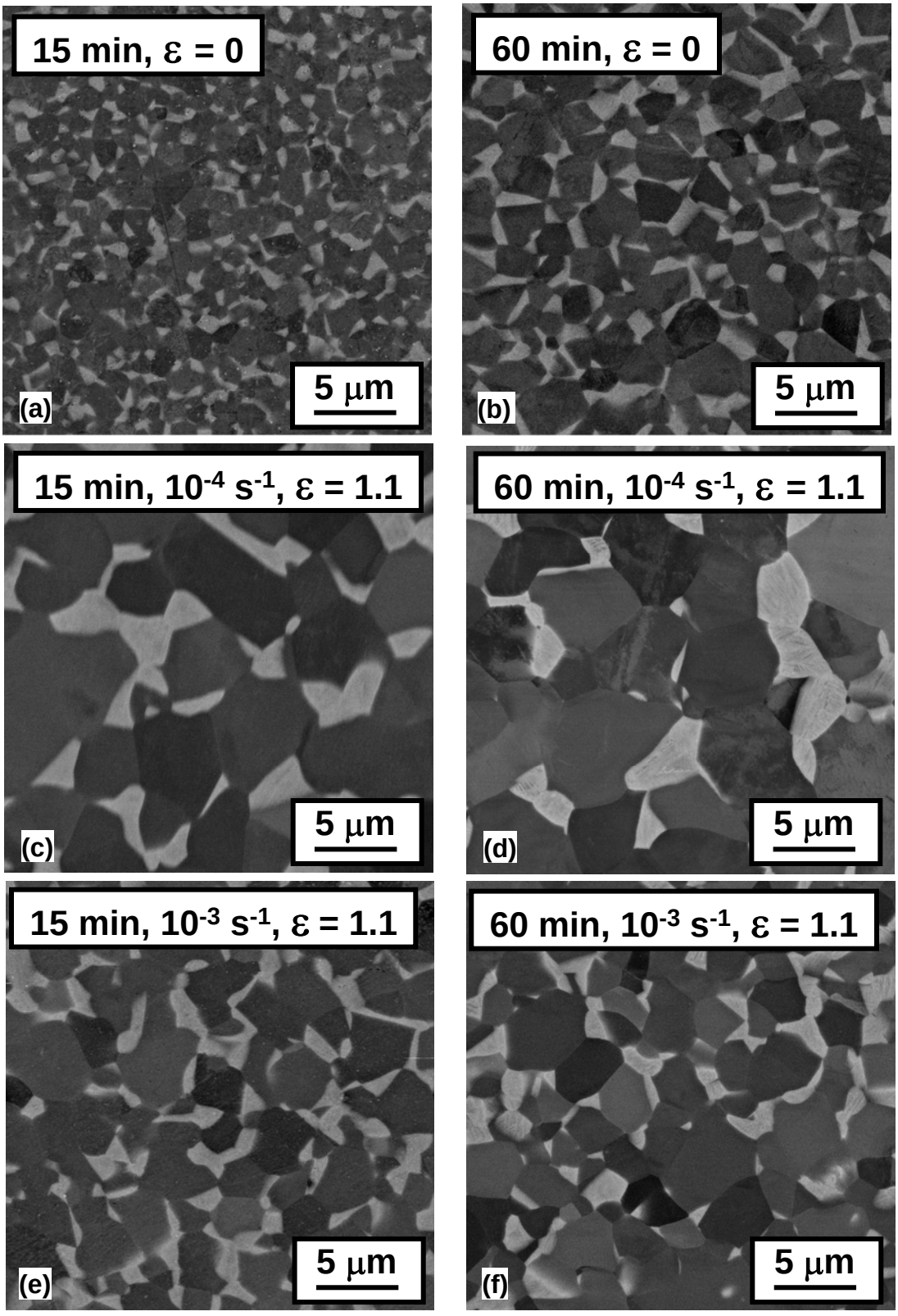

Figure 7. Backscattered electron images of microstructures developed in UFG Ti-6Al-4V at 815°C during (a, b) static heat treatment or (c-f) deformation to a true axial strain of 1.1 following preheating. The soak/preheat time was (a, c, e) 15 min. or (b, d, f) 60 min., and the imposed strain rate was (c, d) 10^{-4} s^{-1} or (e, f) 10^{-3} s^{-1}. The compression axis is vertical in all micrographs.

(a)

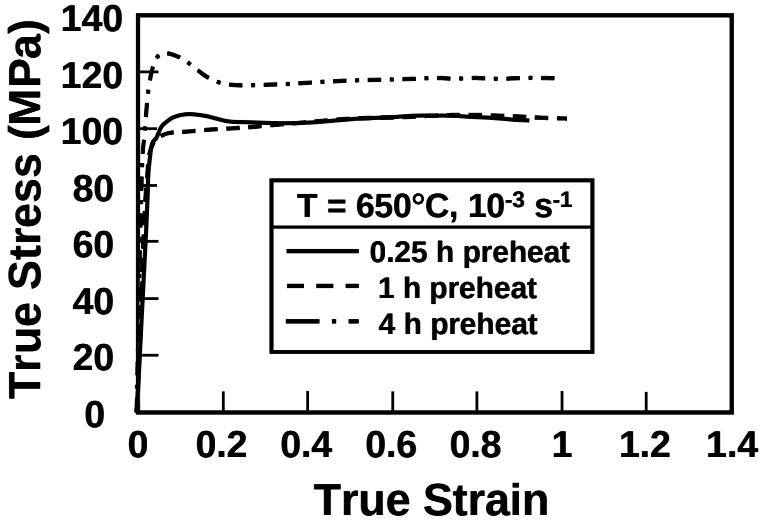

(b)

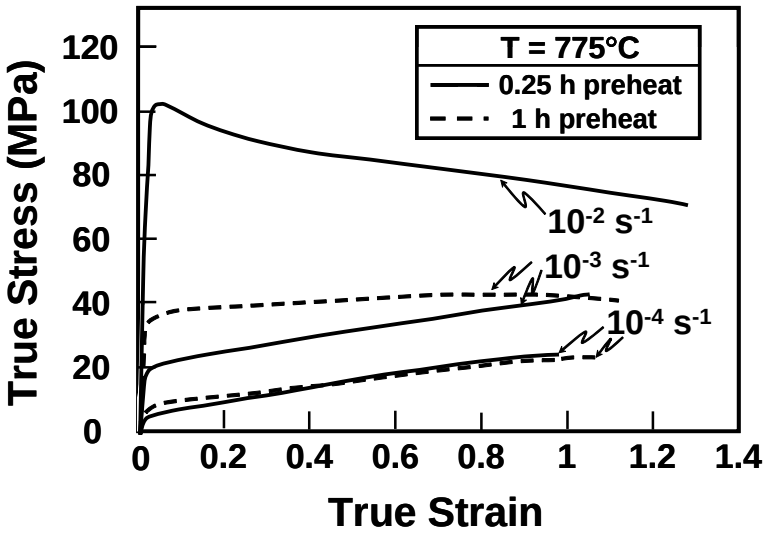

(c)

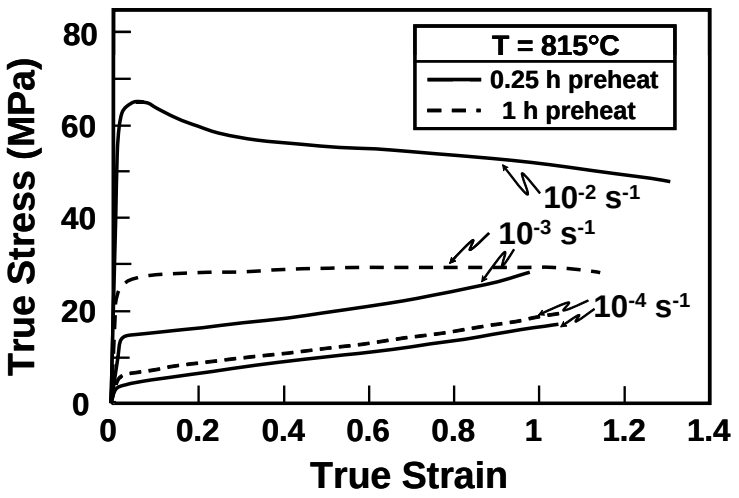

Figure 8. Friction-corrected flow curves for UFG Ti-6Al-4V preheated for 15 or 60 minutes and deformed at strain rates of 10^{-4}, 10^{-3}, or 10^{-2} s^{-1} at (a) 650°C, (b) 775°C, or (c) 815°C.

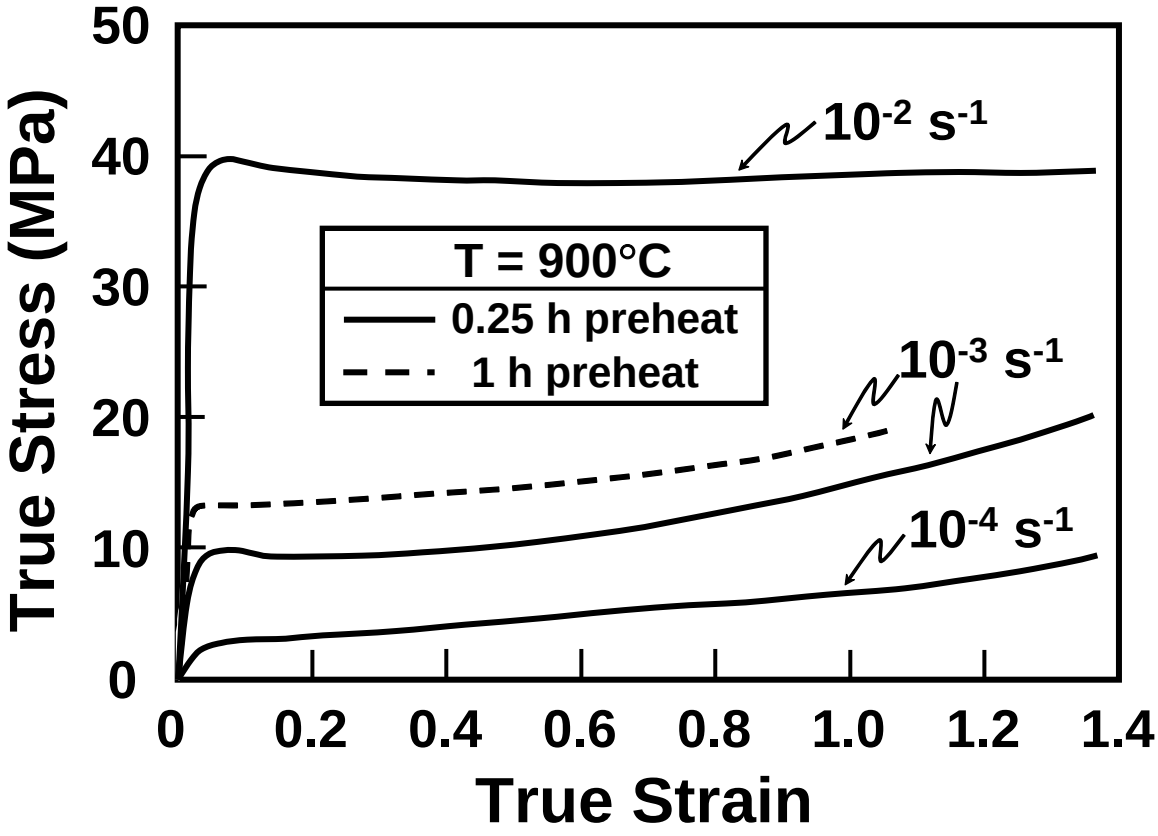

Figure 9. Friction-corrected flow curves for UFG Ti-6Al-4V preheated for 15 or 60 minutes and deformed at strain rates of 10^{-4}, 10^{-3}, or 10^{-2} s^{-1} at 900°C.

(a)

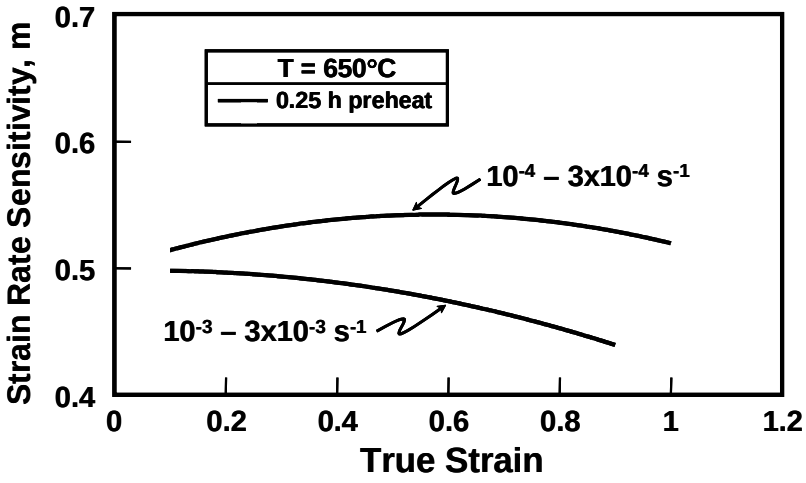

(b)

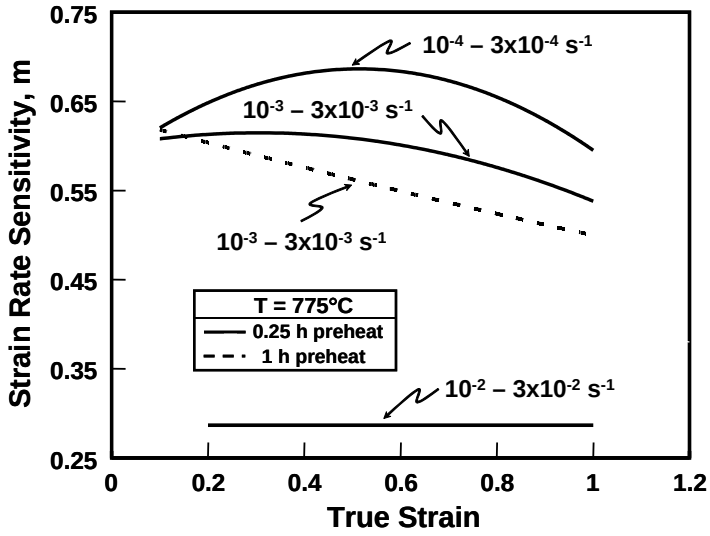

(c)

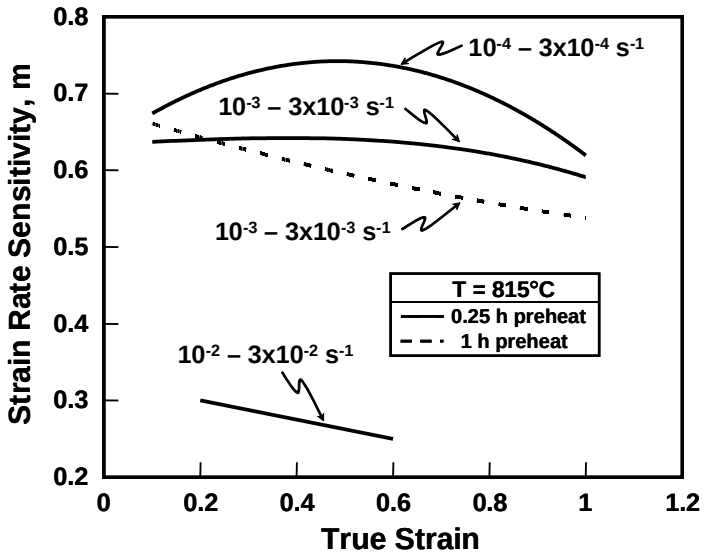

Figure 10. Strain-rate-sensitivity measurements for UFG Ti-6Al-4V from jump tests at (a) 650°C, (b) 775°C, or (c) 815°C.

(a)

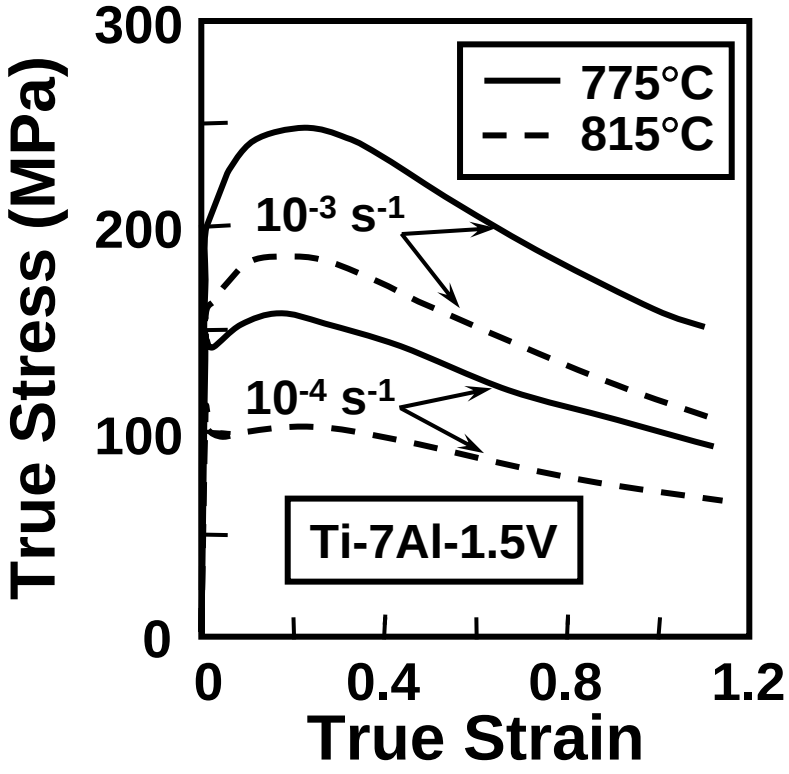

(b)

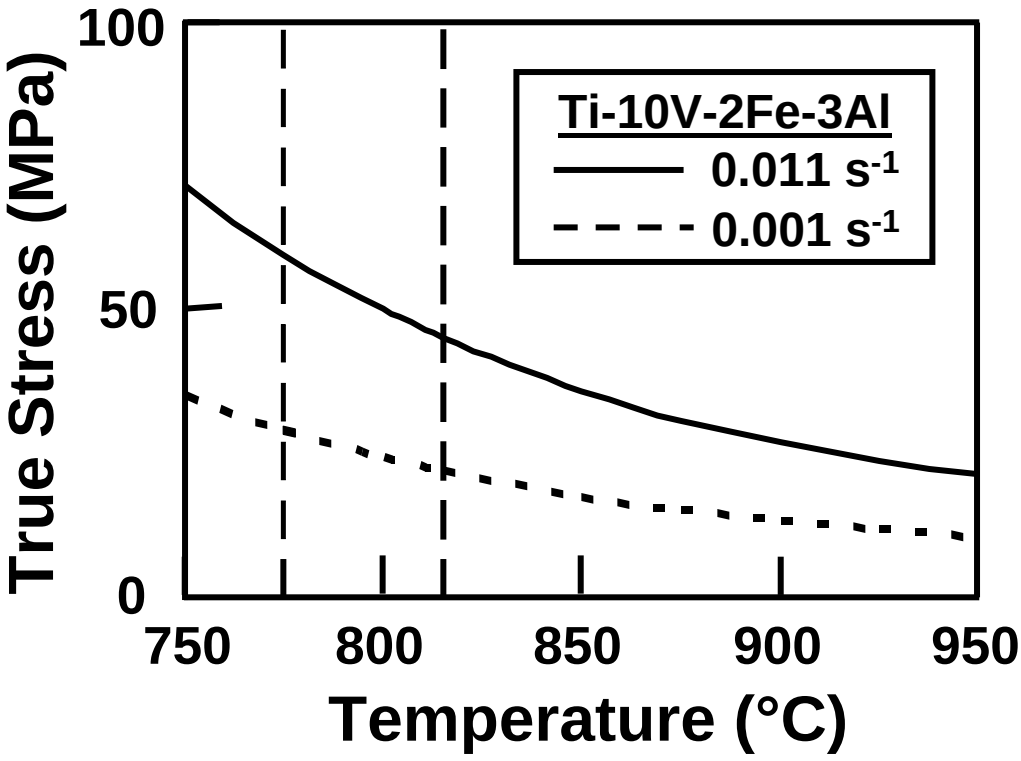

Figure 11. Flow stress data for (a) the single-phase alpha alloy Ti-7Al-1.5V with a grain size of ~75 μm [32] and (b) the beta titanium alloy Ti-10V-2Fe-3Al with a grain size of ~10 μm [33].

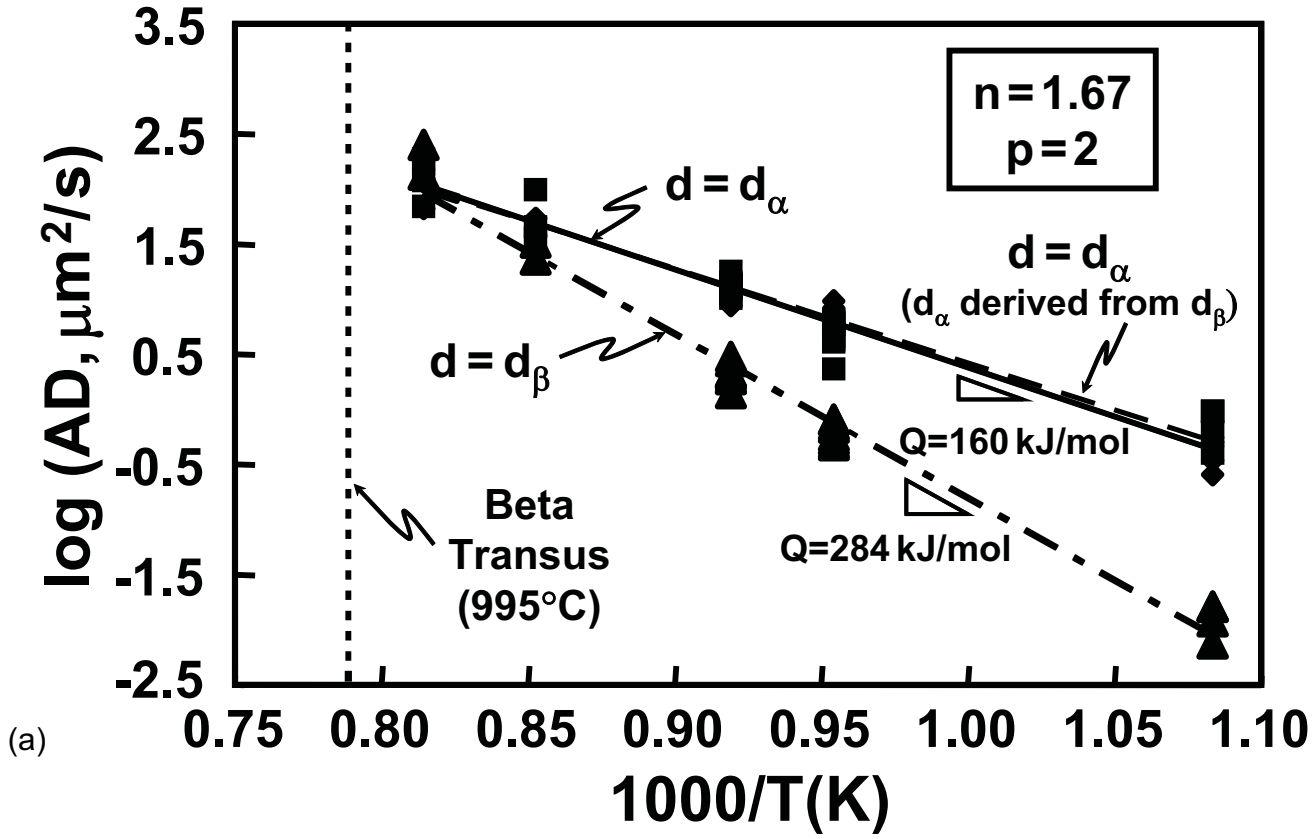

(a)

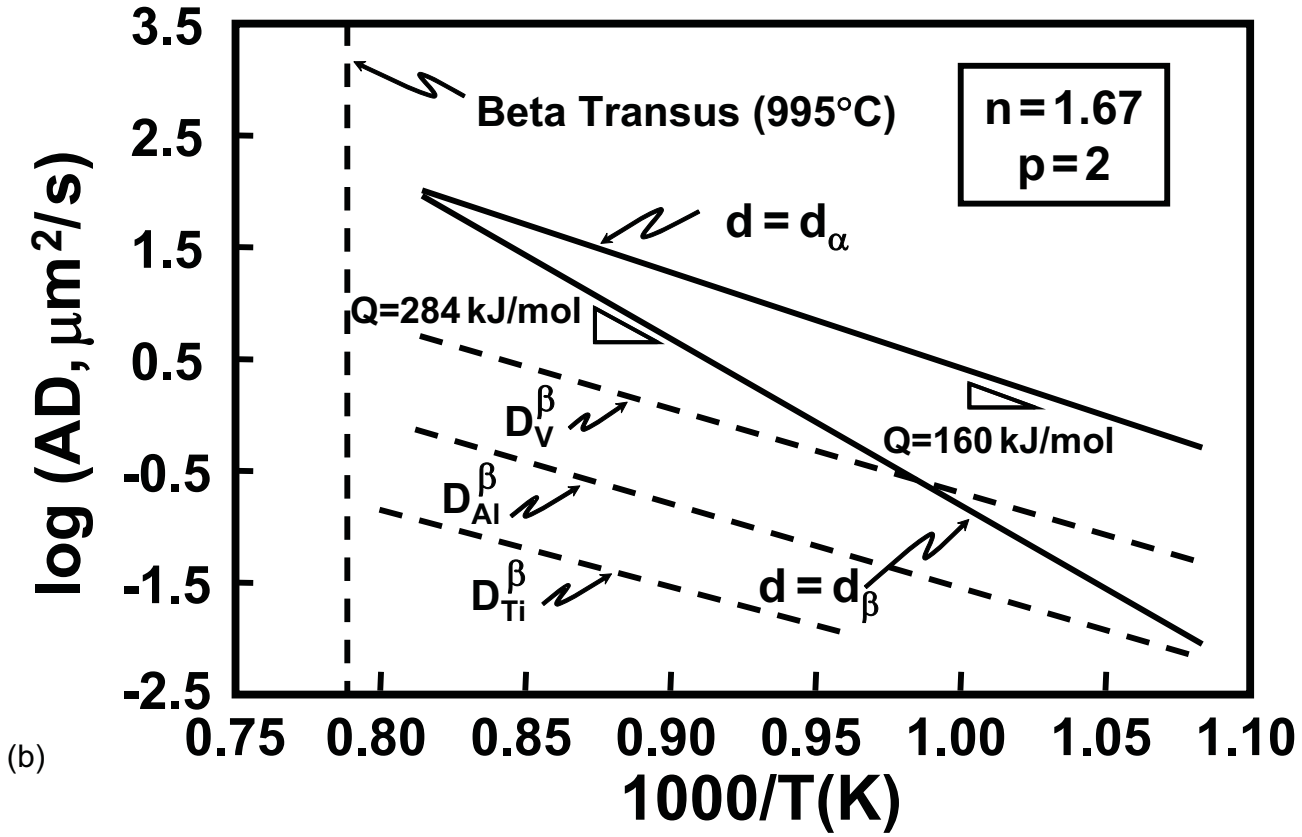

(b)

Figure 12. Semilog plots used to determine the deformation mechanism during superplastic flow of ultrafine Ti-6Al-4V: (a) AD vs 1/T using $d = d_\alpha$ or $d = d_\beta$ and (b) a comparison of AD measurements with literature data for solute and self diffusion in beta titanium.